HYDROXYL RADICAL CREATION USING HYBRID IRON OXIDE-OZONATION

KINETIC DEGRADATION OF SALICYLIC ACID BY HYDROXYL RADICAL CREATION USING A HYBRID IRON OXIDE-OZONATION NANOPARTICLE SYSTEM

By
FREESIA A. WAXMAN, B.ENG

A Thesis

Submitted to the School of Graduate Studies

in Partial Fulfillment of the Requirements

for the Degree

Master of Applied Sciences

McMaster University

MASTER OF APPLIED SCIENCE (2009)
Civil Engineering
McMaster University
Hamilton, Ontario

TITLE: Kinetic Degradation of Salicylic Acid by Hydroxyl Radical Creation Using a Hybrid Iron Oxide-Ozonation Nanoparticle System
AUTHOR: Freesia A. Waxman
SUPERVISOR: Dr. Susan J. Masten
NUMBER OF PAGES: 38

Acknowledgements

I would sincerely like to thank my supervisor, Dr. Susan Masten, and her husband, Dr. Simon Davies for all of their assistance over the years. I am incredibly grateful to all of my family and friends for their continuing support, especially Jamie, who kept me motivated and positive whenever things were not going the way I had planned. I would also like to thank my Mom and Dad for always knowing just how hard to push me without forcing me in one direction or another, and my sisters for always making me laugh. Lastly, I would like to thank my Bubba for her generous support throughout my University education, financial and culinary alike.

Contents

List of Figures

List of Acronymns

2,3-DHBA - 2,3-dihydroxybenzoic acid
2,5-DHBA - 2,5-dihydroxybenzoic acid
COD - Chemical Oxygen Demand
CS - Control Solution
DBPs - Disinfection By-products
ED - Electro dialysis
Fe_2O_3 - iron oxide
HCLA - Hydrochloric Acid
HPLC - High Performance Liquid Chromatography
kPa - Kilo Pascals
MF - Microfiltration
μM - Micro Molar
MWCO - Molecular weight cufoff
NF - Nanofiltration
O_3 - Ozone
$^{\bullet}$OH - Hydroxyl radical
RO - Reverso osmosis
SA - Salicylic Acid
SAO - Salicylic Acid Only (no potassium phosphate)
t-BuOH - Tertiary Butyl Alcohol
THMs - Trihalomethanes
TOC - Total Organic Carbon
UF - Ultrafiltration

Chapter 1

Background

1.1 Introduction

Clean water is a basic human right, and one that most of us take for granted in Canada. While filtration is commonly employed in surface water treatment processes such as granular media filtration, this method is probabilistic due to the variation in void size and some contaminants may slip through (EPA Membrane Filtration Manual, 2005). Membrane filtration represents a barrier with no disinfection by-products (DBPs) created from the reaction of harsh chemicals used to inactivate pathogens. The lack of chemicals required for disinfection purposes cuts down on operating costs, making membrane filtration an attractive alternative for water treatment. The permeability of a membrane depends on the size of the pores. Any particle, including pathogens, which are too large to pass through the membrane pores are separated and accumualte on the inlet side of the membrane while the rest of the solution passes through to be further processed. There have been significant technological advances ever since its inception for desalination in the 1960s (EPA Membrane Filtration Manual, 2005).

The main disadvantage of membrane filtration is fouling, which results in significant increases in the energy required to force water through the membrane as contaminants gradually accumulate on the surface. During the filtration process filtered particles clog the pores of the membrane and reduce the filtration efficiency. Fouling results in the need to backwash clean water through the membrane to remove accumulated foulants. The need to backwash membrane systems results in high energy demands and uses clean water supplies. Different types of membrane filtration such as nanofiltration (MF), ultrafiltration (UF) and microfiltration (MF) differ due to the pore sizes of the membranes. Typical operating ranges for microfiltration membranes range from 0.08 - 2.0 μm, while ultrafiltration membranes range from 0.005 - 0.2 μm and nanofiltration has operating ranges of 0.001 - 0.01 μm (Metcalf & Eddy, 2003). Membrane processes may also be classified as reverse osmosis (RO) with

operating ranges from 0.0001 - 0.001 μm, dialysis and electrodialysis (ED). MF and UF processes separate contaminants through sieving, whereas NF and RO processes use a diffusive mechanism in which ionic compounds may pass through the membrane by diffusion as well as sieving (Metcalf & Eddy, 2003). Membranes are usually defined by their molecular weight cutoff (MWCO) in Daltons, which is the molecular weight of the smallest material that is unable to pass through the membrane (Metcalf & Eddy, 2003).

There are two main configurations for membrane filtration processes, dead end and cross-flow. In dead-end filtration the water flows perpendicular to the membrane, whereas in the cross-flow filtration design the water flows parallel to the membrane. Figure 1.1 provides an example of a typical direct feed MF or UF membrane operation. Membranes can be made from various polymers as well as ceramic materials. Ceramic materials are much more resistant to degradation by compounds such as ozone and are also able to operate under a wider temperature range than polymer membranes. Ceramic membranes also boast more structural strength than their polymer counterparts.

Research conducted by Karnik et al. (2005a, 2005b and 2007) has focused on a hybrid ceramic-ozonation membrane filtration system that eliminates fouling and also significantly decreases the harmful disinfection by-products that typically accompany ozonation and chlorination processes. It has been proposed that fouling of the system was avoided through the oxidation of natural organic matter via the catalyzed (more rapid) degradation of ozone, which resulted in the creation of hydroxyl and other secondary radicals.

The surface of the membrane in the experiments performed by Karnik et al. (2005a, 2005b and 2007) was coated with layers of iron oxide, which was demonstrated to have catalytic properties and resulted in no fouling of the membrane. Studies conducted in 2007 by Karnik et al. used salicylic acid (SA) as a model contaminant to examine the role of hydroxyl radicals in the system. Similaryly, the purpose of this study was to observe the degradation kinetics of a suspension of salicylic acid and to monitor the evolution of the by-products 2,3-dihydroxy benzoic acid (DHBA) and 2,5-DHBA to confirm oxidation through hydroxyl radical formation as the main degradation pathway. Karnik et al. (2009) also evaluated the effect of surface area by examining the effect of the number of iron oxide layers on the formation of disinfection by-products (DBPs). The effect of available iron oxide surface area was also therefore also investigated in this study by analysing suspensions of various concentrations/surface areas of iron oxide.

The changes in composition of a mixture containing 20 mg/L salicylic acid (SA), phosphoric acid, and potassium phosphate were studied over a 4 hour time span

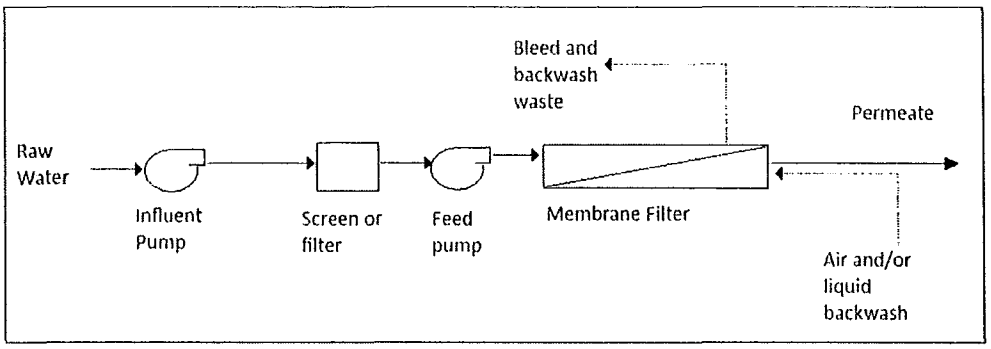

Figure 1.1: Direct Feed Operational Mode for MF and UF Membrane Processes (Adapted from Metcalf & Eddy, 2003)

under various conditions. The degradation kinetics were monitored during the 4-hour experiments for two different suspensions, one having a pH of 8 and the other a pH of 3. Analyses of the solutions was conducted at pH 3 and pH 8 to investigate the effects of ozone decomposition. At high pH values there are more hydroxide ions present in the solution/suspension, which leads to increased ozone decomposition rates as hydroxide ions have been shown to promote the decomposition of ozone. At a lower pH there are much fewer hydroxide ions present and as a result the decomposition of ozone is slower. The contents of the mixture were analyzed by high performance liquid chromatography (HPLC) to quantify the concentrations of salicylic acid and its by-products.

Several studies have been performed to investigate the catalytic effect of various minerals and metal oxides on ozone decomposition and the degradation of organic substances (Einaga and Ogata 2009, Devulapelli 2008, Lin and Lin 2008, Karnik et al. 2007, Allemane et al. 1993). It has been proposed that surface-bound hydroxide ions are capable of reacting with ozone, thereby increasing the rate of ozone degradation for a manganese catalyst (Ma and Graham, 1999). Studies conducted on granular iron oxide by Lin and Gurol (1998) revealed that the iron-oxide catalyst was responsible for reducing the residual ozone concentration. Karnik et al. (2007) showed that SA was not degraded to any appreciable extent at pH 2.5-3.0 when the iron oxide-coated membrane was not present in the system, indicating that hydroxyl radicals were not formed in sufficient quantities to promote degradation of the contaminant. Forty percent (40%) of the SA was degraded by ozone at pH 7.0-8.1. In studies conducted by Xing et al. (2008) with a magnesium oxide catalyst and mesoporous zirconia support, the metal oxide was shown to catalyze the degradation of 2,4-dichlorophenoxyacetic acid through the enhanced degradation of ozone into hydroxyl radicals. Researchers are still not entirely certain of the exact reaction mechanism behind the catalytic degradation observed in with various metal oxide

catalysts (Xing et al. 2008, Karnik et al. 2007), but current theories postulate that the formation of Lewis acid sites and surface charge play a key role (Yang et al. 2009, Xing et al. 2008).

Phosphate has been used extensively in experiments to control pH, yet the effects of phosphate as a catalyst itself are rarely elucidated. Phosphate is capable of acting as a hydroxyl radical scavenger, as was illustrated by Staehelin and Hoigné (1985). A few authors have noted reduced rates of oxidant decomposition (Bower and Miller 2002) as well as increased quantities of degraded contaminant (Andreozzi et al. 1998a) when phosphate was utilized in solution as a pH buffer. Yi et al. (2003) found that at neutral pH the oxidation reaction for an ozone system was strongly inhibited by the presence of a phosphate buffer.

Bower and Miller (2002) observed that ozone decomposition rates were much greater in the absence of a phosphate buffering solution. They proposed that increased degradation rates were due to the ability of phosphate to act as a hydroxyl radical scavenger. Masten et al. (1996) noted decreased contaminant removal rates when experiments were performed at pH 11.7 compared to those conducted at pH 8.0 and suggested that hydrogen phosphate may have scavenged hydroxyl radicals, thereby reducing the oxidative capacity of the solution. Hoigné and Bader (1976) chose to work with a sodium phosphate buffer in order to avoid buffering solutions that would react with ozone.

Experiments performed by Andreozzi et al. (1998a) showed that in the absence of the phosphate buffer ozone decay rates were found to be 3.4 times faster for virgin filter media and 1.5 times greater for hydrous iron oxide coated sand. The ozone alone results showed a small decrease in the ozone decay rate when phosphate was present as well. The use of a phosphate buffer at pH 3.0 did not result in any noticeable contaminant degradation. Leitner et al. (1999) were unable to use a phosphate buffer during mass balance experiments because it adsorbed to the catalysts.

Solid tripotassium phosphate has been shown to act as a catalyst for phase-transfer alkylation reactions by Qafisheh et al. (2007). Potassium phosphate was also proven to be an effective catalyst for the Knoevenagel condensation reactions (Li, 2000).

Tertiary butyl alcohol or tert-butyl alcohol (t-BuOH) has been used as a hydroxyl radical probe (for example, see Xing et al. 2008, Karnik et al. 2007, Andreozzi et al. 1996). Masten et al. (1996) used 10 mM empht-BuOH at a pH of 2 in order to investigate reactions by molecular ozone.

1.2 Ozone Degradation

While ozone is a relatively strong oxidizer it is also a rather selective one, meaning that there are a limited number of compounds that can be directly oxidized by molecular ozone (Hoigné and Bader 1976). By combining ozonation with various heterogeneous metal oxide materials, researchers have been able to enhance the formation of hydroxyl radicals (Avramescu et al. 2009). OH radicals are formed through the degradation of ozone and are termed non-selective oxidants (Legube & Leitner 1999). With an even greater oxidative power than ozone, advanced oxidation processes utilize OH radicals and radical intermediates to degrade a wide range of pollutants (Masten et al. 1996).

Contaminants may undergo direct oxidation by molecular ozone and could also be subjected to oxidation by radicals resulting from ozone decomposition. In catalytic systems there are even more removal pathways possible for contaminant degradation. Oxidation may take place on the catalytic surface, the pollutant might adsorb to the catalyst, or the compound may be oxidized by radicals formed through the catalytic degradation of ozone (Avramescu et al. 2009).

There are many steps along the path of ozone degradation and hydroxide ions play a key role. The first step that sets off the chain reaction can be initiated by the interaction of ozone with hydroxide ions (Legube & Leitner 1999), causing hydroxide ions to catalyze the decomposition of ozone (Hoigné and Bader 1976). This means that at higher pH values ozone decomposition rates generally increase, as has been observed by many researchers (e.g., Avramescu et al. 2009, Masten et al. 1996, Hoigné and Bader 1976). Other steps during ozone decomposition include propagation and chain breakdown mechanisms. Just as the radical chain reactions may be initiated, they can also be promoted or inhibited. Ozone is a compound which actually promotes its own degradation. Primary and secondary alcohols and humic substances have been found to also be capable of acting as promoters, while tertiary alcohols and carbonate act as inhibiting compounds (Legube & Leitner 1999). Ozone may also decompose into superoxide ions which can in turn result in the formation of hydrogen peroxide, H_2O_2 (Hoigné and Bader 1976).

Experiments with various metal catalysts have shown that aqueous ozone concentrations generally reach a steady state and are dependent upon pH (Avramescu et al. 2009, Masten et al. 1996). Sreethawong et al. (2008) has also shown that as the ozone generator power increased the removal efficiency of organic matter correspondingly increased as well. At lower generator power settings less ozone can be produced by passing air through a high voltage discharge, which results in lower removal efficiencies.

In the past, chlorine was the disinfection agent of choice for most drinking water treatment facilities in Canada, the U.S. and England. Ozone is gaining ground as a disinfection method due to the fact that when chlorine reacts with natural organic matter (NOM) it results in the formation of disinfection by-products such as trihalomethanes and halo acetic acids, which are known, or potential, carcinogens. When ozone reacts with NOM the resulting disinfection by-products are aldehydes, ketones and ketoacids, some of which are also carcinogenic (Paode et al. 1997, Mackenzie and Masten 2004). Bromate formation is another concern with ozonation systems. This ozonation by-product is a known carcinogen (AWWA 1993) that can result from the interaction of ozone with bromide (Song et al. 1997). OH radicals have been shown to significantly increase the rate of formation of bromate (Gunten and Hoigné 1994). Metals such as zero-valent iron impregnated with copper have been shown to disrupt the formation of bromate in contaminated groundwater systems (Xie and Shang 2006).

A draw-back of ozonation systems is that ozone is an unstable molecule that degrades quickly into molecular oxygen and it therefore needs to be generated at the point of application. A common method of producing ozone is by discharging a high voltage through air or pure oxygen which is very energy intensive and therefore expensive.

1.3 Metal Oxides

Nickel, alumina, copper and cobalt were tested for their catalytic properties in a study by Avramescu et al. (2009) who found that the addition of these various metals reduced the contaminant (acid red 88 dye) degradation time by half compared to ozone alone. Some of the metals were found to exhibit a high contaminant adsorption capacity which led to two different reaction mechanisms for ozone degradation; adsorption and subsequent surface oxidation or oxidation in the bulk solution. The catalysts with a low contaminant adsorption capacity were assumed to degrade the dye through the formation of hydroxyl radicals due to the catalytic decomposition of ozone or through reactions with molecular ozone. The ozone degradation theory is supported by findings that the low contaminant absorption catalysts exhibit a steady decrease in total organic carbon (TOC) and COD with reaction time whereas the higher contaminant adsorbant catalysts show a marked increase in parameter removals followed by a slower decline in values with time (Avramescu et al. 2009). This may be due to differences in the reactivity of the sites on the metal oxides. The more reactive sites would react first during the rapid contaminant degradation in the beginning. As those sites are exhausted, the less reactive sites would react with the contaminant and the degradation would continue, but at a slower rate. Interestingly, pH was found to have little effect on the contaminant degradation rate regardless of catalyst type.

Molybdenum oxide was used as a catalyst promoter in ozonated copper oxide catalyst experiments performed by Devulappelli et al. (2008). They found that an increase in the number of acid sites was achieved through the addition of molybdenum oxide, which in turn led to the formation of more complete oxidation products. Reduced metals have also been found to act as initiators for the degradation of ozone (Legube & Leitner 1999).

A study conducted by Sreethawong et al. (2008) revealed that iron oxide-coated alumina balls packed into a reactor column catalyzed the degradation of ozone, resulting in a six-fold increase in the color removal efficiency. In a comparative study by Mitchell et al. (2007) researchers found that a combination of 15 wt% Fe_2O_3 on alumina oxide outperformed lower and higher loadings of Fe_2O_3 as well as 20 wt% cerium oxide-coated Al_2O_3, Al_2O_3, and MCM-41 (silica material) during ozonation tests.

Xing et al. (2008) investigated the surface charge effects of manganese oxide (MnOx) towards ozone degradation compared to the support material, mesoporous zirconia, and demonstrated that surface potential increased both with increasing pH as well as with the addition of a MnOx coating, increasing the activity of the solutions. It was observed that the point of zero charge (PZC) increased with the addition of MnOx. In solutions with a pH above the PZC the surfaces became negatively charged and it was proposed that ozone preferentially reacted with the charged surface instead of the model compound, 2,4-dichlorophenoxyacetic acid (Xing et al. 2008).

While investigating the degradation of various pharmaceutical compounds with manganese oxide on mesoporous and nonporous alumina supports, Yang et al. (2009) found that one pharmaceutical in particular (phenazone) never adsorbed to the MnOx catalyst and proposed that the compound therefore must have been degraded in the bulk solution by the catalytic formation of hydroxyl radicals. The authors measured the zeta-potential of the synthetic mesoporous alumina (MA) support and found that it had the highest isoelctric point of all of the tested supports (commercially mesoporous alumina, MA and nonporous alumina), with a pH of 8.6. When coated with MnOx, the MA support also exhibited the greatest removal efficiencies for the pharmaceuticals and had the largest measured surface area, which led the authors to conclude that properties such as increased surface area and surface charge could be responsible for higher catalytic activity. Oxide species identified on the catalytic surface were assumed to function as active sites for the ozonation of the pharmaceutical compounds. The addition of MnOx resulted in the alumina surface hydroxyl groups being utilized as active sites as well.

Mitchell et al. (2007) claim that degradation of the model contaminant DDMP (dimethyl methylphosphonate) was limited by the number of available surface reaction sites for a variety of metal oxides. These results also indicate that contaminant removal could be increased by increasing the available metal oxide surface area.

Sulzberger et al. (1989) proposed that surface Fe(III) could act as a centre for ligand attachment, functioning as a Lewis acid. The authors also show how phosphate molecules may become bound to iron oxide surface in the presence of water, leaving surface OH groups which may be exchanged for other ligands. The solid oxide surface reacts most effectively with molecules that are adsorbed to the surface (Sulzberger et al. 1989).

1.4 Salicylic Acid

Salicylic acid (SA) is most commonly known for its use in cosmetic creams and its relation to the common painkiller ingredient acetylsalicylic acid. This aromatic hydrocarbon was chosen as a model contaminant due to the fact that it does not significantly react with molecular ozone, yet it is readily degraded by hydroxyl radicals (Legube and Leitner 1999, Punchard and Kelly 1996). Alternative compounds, such as pentanoic acid, have also been used as hydroxyl radical probes due to their similar reaction mechanisms with ozone and OH radicals (Masten et al. 1996).

In previous studies by Karnik et al. (2007), it was demonstrated that SA degraded into the by-products 2,3-DHBA and 2,5-DHBA over the course of 4 hours when subjected to ozonation due to the formation of hydroxyl radicals. Other researchers have reported SA degradation by-products such as maleic acid and catechol (Albarran and Schuler 2003, Jen et al. 1998). SA was shown to be non-reactive with molecular ozone in the pH range 2.5 - 3.0 and was not significantly (within 5% std. deviation) sorbed to the membrane surface during ozonation tests. In the higher pH ranges (7.9 - 8.1) the membrane-only experiments did exhibit SA concentration decreases which were assumed to occur due to membrane adsorption. The salicylate ion was therefore proposed to be more adsorbent than the protonated form of SA. Ozone was found to degrade SA much more rapidly at the higher pH than at pH 2.5-3.0, due to the fact that hydroxide ions promote ozone degradation.

pH was shown to have a significant impact on pollutant removals in a study conducted by Masten et al. (1996) that investigated the oxidation of chlorinated benzenes, including pentanoic acid, which reacts with ozone in a similar manner to SA. Optimal removal of the compound was found to occur between pH 7.0-8.5, while results obtained at pH 2.2 were postulated to have lower removal efficiencies due to

the decreased decomposition rate of ozone in lower pH ranges (Masten et al. 1996).

1.5 Iron Oxide-coated Ceramic Membrane Filtration

1.5.1 Introduction

Membrane filtration is gaining acceptance as a means of disinfection for drinking water treatment due to the concern about chlorine resistant microorganisms and subsequent disinfection by-products (EPA Membrane Manual 2005). Catalytic membrane filtration systems in combination with ozonation have been proven to increase the degradation of various model contaminants. Common metal-oxide catalysts include iron(III) oxide, titanium dioxide, aluminum oxide and manganese oxide (Andreozzi 1998b, Leitner et al. 1998, Lin 1998).

Karnik et al. (2005b), in a study of hybrid ozonation-ceramic membrane filtration, found that decreasing the pH of the water to be treated from 8 to 4 resulted in increasing aqueous ozone levels. It was also discovered that there was a threshold ozonation level beyond which no additional permeate flux recovery was gained. The hybrid ozonation-membrane system greatly reduced the concentration of disinfection by-products formed, namely the total trihalomethanes (TTHMs) and halo acetic acids (HAAs) (Karnik et al. 2005b). Subsequent research by Karnik et al. (2009) investigated the effect of the number of iron oxide coatings on ozonated membrane performance and found that 40 layers resulted in significant dissolved organic carbon (DOC) removal when compared to the uncoated membrane or up to 60 layers of 4-6 nm Fe_2O_3 particles iron oxide nanoparticles. It was postulated that water quality improved with increasing iron oxide layering up to the 40 layer mark because of increased membrane surface area achieved through micron-scale surface undulations and coarsening of pores, both of which resulted from the heat treatment process. X-ray diffraction characterization of the membranes showed that α-Fe_2O_3 was present after sintering at 900°C. Iron oxide-coated membranes were shown to be significantly more effective than either the uncoated membranes or ozone alone for the degradation of the model contaminant SA, with up to 95% removal in 4 hours (Karnik et al. 2007). Hydroxyl and other radical species formed through indirect oxidation reactions were postulated to be responsible for the increased SA degradation rates observed in the iron oxide system (Karnik et al. 2007). The metal oxide coating was also found to affect the dissolved ozone levels, decreasing aqueous ozone concentrations by more than 40% compared to the uncoated experiments.

1.5.2 Postulated Degradation Mechanisms

Sreethawong et al. (2008) used the following equations to describe the catalytic degradation of ozone by iron oxide (Hart et al. 1983, Logager et al. 1992, Wedley & Waite 2004):

$$Fe^{3+} + H_2O \rightarrow Fe^{2+} + H^+ + {}^{\bullet}OH \tag{1.1}$$

$$Fe^{2+} + O_3 \rightarrow Fe^{3+} + O_3^- \tag{1.2}$$

$$O_3^- \rightarrow O^- + O_2 \tag{1.3}$$

The equations show how it would be possible for Fe_2O_3 to act as a true catalyst and not be consumed during the reactions while aiding the degradation of ozone to form hydroxyl radicals. Sreethawong et al. (2008) found that the form of the iron oxide remained unchanged after numerous ozonation tests were performed and that the effluent pH did not change significantly.

In aqueous systems, metal oxides have been shown to dissociate water molecules through adsorption, resulting in surface H^+ groups attached to oxygen sites and OH- groups on metal sites forming Lewis acid reaction sites (Joseph et al. 2000). The presence of strong Lewis acid sites leads to the adsorption and subsequent decomposition of Lewis bases such as ozone (Yang et al. 2009). Researchers have also discovered that when ozone was added to MnOx/alumina suspension the amount of surface hydroxyl groups greatly increased due to the catalytic decomposition of ozone which resulted in more OH^- groups available to hydrogen bond with the catalytic surface (Yang et al. 2009).

The catalytic ability of nano-sized iron oxides was investigated by Wang et al. (2007) who found that by raising the temperature and/or ozonation dosage, the activity of iron oxide could be increased. It was also proposed that an active complex consisting of a Lewis acid (O^-Fe^{3+}) may be formed on the oxide surface due to ozone decomposition for gaseous systems (Wang et al. 2007). The active O^-Fe^{3+} site may be responsible for the catalytic decomposition of ozone as the Lewis base would be attracted to the surface bound Lewis acid site. Dhandapani and Oyama (1999) and Karnik et al. (2007) also suggested that atomic oxygen (O^-) was formed on the surface of α-Fe_2O_3 when ozone was degraded. O^- is a strong oxidizer which acts as a Lewis base and could contribute to the enhanced contaminant removal ability of iron oxide by attracting Lewis acid compounds. Atomic oxygen could also react with surface oxides to produce superoxide anions which could then react with aqueous ozone to generate ozonide anion radicals (O_3^-) (Karnik et al. 2007). At pH 8 the O_3^- could produce $^{\bullet}$OH which could subsequently degrade SA.

Chapter 2

Experimental Setup

2.1 Reactor Design

Experiments were conducted in a semi-batch system (continuous ozone/oxygen gas supply, fixed volume of aqueous sample), consisting of an ozone generator (Ozone Solutions, USA Model #HTU500AC), a UV-VIS spectrophotometer for gaseous ozone analysis (Shimadzu UV-1201), as well as a 5% potassium iodide (KI) trap to destroy residual ozone. The reactor is a 1.5L glass vessel and all experiments were performed at $25 \pm 1°C$. Ozone was delivered into the solution by means of a ceramic bubbler located near the bottom of the reactor. The reaction vessel was placed on a stir plate set at a constant stirring level. Refer to Figure B.1 for a picture of the reactor vessel. Gaseous ozone was measured spectrophotometrically at $\lambda = 258nm$ using a corresponding extinction coefficient of $\epsilon = 3000M^{-1}cm^{-1}$(Nowell et al. 1988). The indigo colorimetric Standard Method 4500-O_3 B (Bader and Hoign, 1981) was used to determine aqueous ozone concentrations within the solution. Figure 2.1 shows a schematic of the reactor system.

2.2 Materials

The SA used was 99% pure ACS grade ReagentPlus (Sigma-Aldrich, USA). 99.0% pure 2,3-DHBA was obtained from Sigma-Aldrich (St. Louis, USA) and 99.0% pure 2,5-DHBA from Sigma-Aldrich (Switzerland). Potassium phosphate monobasic ACS grade was purchased from EMD Chemicals Inc. (Darmstadt, Germany), as were sodium hydroxide pellets. 85% phosphoric acid, potassium iodide, tertiary butyl alcohol and 37% hydrochloric acid were purchased from Fisher Scientific (Ontario, Canada). Potassium indigo trisulfonate was purchased from Sigma-Aldrich (St. Louis, USA). Acetonitrile and HPLC grade water were purchased from Caledon Laboratories (Ontario, Canada). The standard solutions were prepared in potassium phosphate (0.1M) solution with 0.07mL of phosphoric acid added. Barnstead

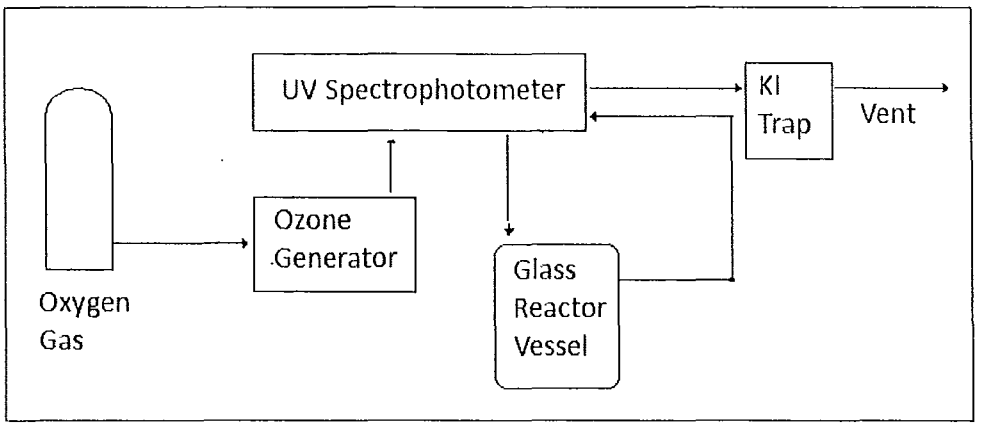

Figure 2.1: Reactor System Schematic

NANOpure water was used for all solutions and reagent stock. Millipore membrane filters (25 mm diameter, 0.45 μm porosity) were used for filtration purposes. Pure oxygen gas (99.999%) was obtained from Vital Aire (Ontario, Canda). 98% pure alpha-phase iron oxide nanopowder (20-50 nm APS) was purchased from Nanostructured and Amorphous Materials Inc. (Texas, USA).

2.3 HPLC

A Varian high performance liquid chromatography system equipped with an Agilent Zorbax SB-C18 4.6 x 250mm 5 μm column, a Varian UV detector, and a Varian auto sampler was used with an eluent flow rate of 1.0mL/min. Eluent A was composed of 0.1% phosphoric acid (85%, Fisher Scientific, Canda) in HPLC grade water and eluent B was HPLC grade acetonitrile. The eluent flows changed from 80% A and 20% B to 50% each after 6 minutes and reverted back to 80% A and 20% B after 12 minutes. The UV detector was set to 210 nm from 0-10.50 minutes and to $300nm$ from 10.51-19 minutes. Injection volumes of 100 μL were used in each analysis. A sample chromatogram is shown in Figures 2.2 and B.2.

2.4 Degradation Conditions

Salicylic acid concentrations in the range of 20-23 mg/L were used in the following experimental suspensions to simulate the typical TOC concentrations found in Lake Lansing, a borderline eutrophic lake in mid-Michigan, which was used in previous studies (Karnik et al. 2007). Aqueous samples were taken from the reactor every 5 minutes for the first half hour and on the hour for the duration of the four-hour experiments. Samples were immediately refrigerated. HPLC analysis was performed

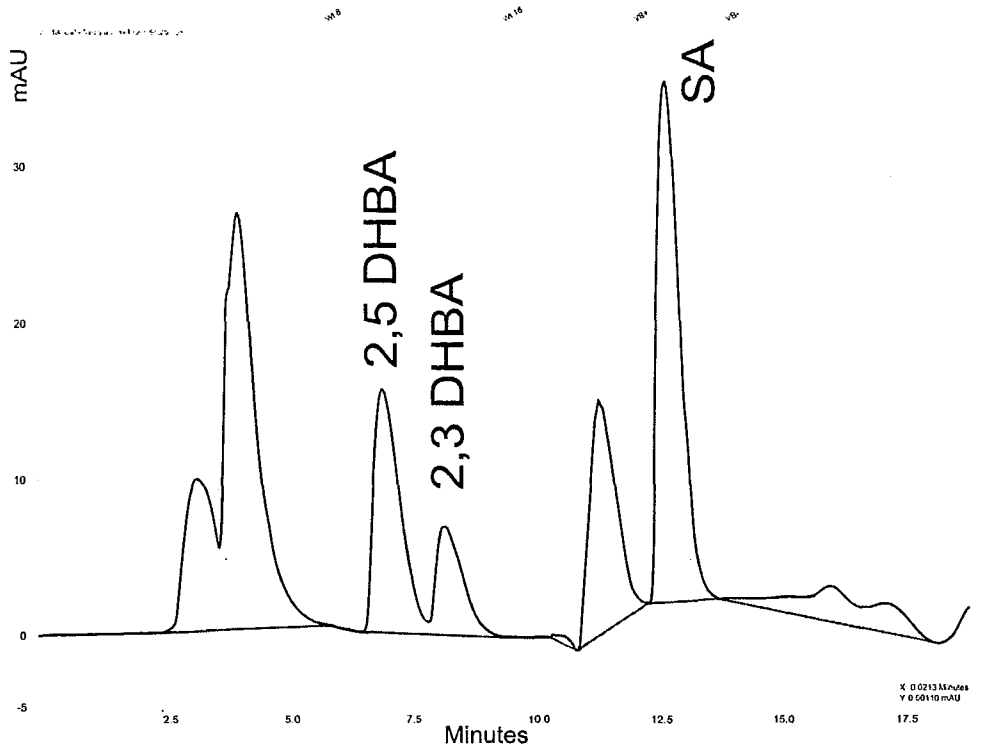

Figure 2.2: Sample Chromatogram from May 17, 2009 SAO with Ozone at 25 Minutes

on the mixture to monitor the disappearance of the target compounds. The experiments were performed at pH 2.8-3.5 and 7.8-8.1. When a hydroxyl radical scavenger was required, tertiary butyl alcohol (t-BuOH) was added to the solution at 0.01M, unless otherwise noted.

A fresh supply of SA (20 mg/L) was prepared daily for each experiment. 2,3-DHBA, 2,5-DHBA and SA HPLC standards were prepared once a week to obtain calibration curves at 5 concentration levels. All pH 8.0 samples were adjusted to pH 3.0 before analysis with ACS reagent grade phosphoric acid.

2.4.1 Adsorption Experiments

Adsorption experiments were performed with 10, 20, 40, 60, 80 and 100 mg/L Fe_2O_3 at both pH 3 (without phosphoric acid) and pH 8 (with phosphoric acid and sodium hydroxide). Oxygen, ozone and potassium phosphate were not added during the adsorption experiments. A 1 litre glass bottle was filled with 20 mg/L SA for pH 3 experiments with the addition of sodium hydroxide and phosphoric acid for pH 8 experiments. Iron oxide nanoparticles were added at concentrations ranging from

0-100 mg/L. The solutions/suspensions were placed on a magnetic stir plate and continuously mixed for the duration of the experiments. The bottles were sealed with Parafilm and samples were taken at 1, 2, 4, 8, and 23 hour intervals for the 100 mg/L experiments to determine an appropriate sampling time. 0-80 mg/L experiments were conducted for 1 hour with samples taken at the beginning of the experiment and at the 1 hour mark. Samples were then analysed by HPLC for SA and by-products 2,3-DHBA and 2,5-DHBA .

2.4.2 High Ozone Experiments - Setting 3

The study consisted of multiple experiments on a SA mixture, each of which was 4 hours in duration. Water samples were spiked by adding 1000 mL of 0.1 M potassium phosphate to achieve a final phosphate concentration of 0.067 M in the treated solution. The pH of the solution was adjusted with the addition of phosphoric acid for the pH 3.0 experiments or with sodium hydroxide for the pH 8.0 experiments. The final volume of each solution was 1.5 L with a SA concentration of approximately 20mg/L. Six types of solutions/suspensions were tested in the experiments as noted in Table 2.1. The control solution contained 20 mg/L SA solution in DDI water with 0.067 M potassium phosphate, phosphoric acid and where appropriate, sodium hydroxide.

Table 2.1: Six Types of Experimental Solutions

Experiment Type	Solution Components	Short Form
1	CS + pure O_2	Control
2	CS + 4 mg/L O_3 gas	O_3
3	CS + 10 mg/L O_3 gas	10 mg/L Fe_2O_3
4	CS + 100 mg/L Fe_2O_3 + O_2	100 mg/L Fe_2O_3
5	CS + 10 mg/L Fe_2O_3 + O_3	10 mg/L Fe_2O_3 + O_3
6	CS + 100 mg/L Fe_2O_3 + O_3	100 mg/L Fe_2O_3 + O_3

**CS = Control Solution*

The influence of the catalyst surface area was investigated for Fe_2O_3. Aliquots of 5 mL were taken from the reactor every 5 minutes for 30 minutes, and then once every hour for the duration of the four hour experiments. Samples were drawn from the reactor with a syringe and filtered through 0.45 μm filter paper to remove suspended iron oxide particles. 2 mL of the filtered sample was analyzed by HPLC and 1 mL of the unfiltered sample was used to determine the aqueous ozone concentration. The HPLC analyses, as well as the aqueous ozone measurements, were all performed in triplicate. The 1 mL aqueous ozone samples were immediately

purged into 24 mL of indigo reagent II solution. Aqueous ozone samples were left for 4-5 hours before being filtered through 0.45 μm filter paper and analysed by a spectrophotometer at 600 nm according to the indigo method (Bader and Hoign, 1981). A blank consisting of 24 mL indigo reagent II and 1 mL of non-ozonated sample water was measured before each aqueous ozone sample to account for errors of the spectrophotometer. Gaseous ozone concentrations were also measured at corresponding time intervals for the duration of the experiments with a UV spectrophotometer at 258 nm via flow-through cells. The inlet gaseous oxygen pressure was set to 55 kPa and the ozone generator was set to 3 on a scale of 1-10 with ten being the highest voltage.

2.4.3 Long-term Experiment

An 8 hour experiment was performed in order to verify that the aqueous and gaseous ozone concentrations had reached steady-state by the 4 hour mark.

2.4.4 Dark Experiment

An experiment was performed in order to verify that photo-oxidation was not responsible for the observed SA degradation behaviour observed during the "high ozone" experiments. For this experiment the reactor was completely wrapped in tinfoil so that the solution would be exposed to no light from the fluorescent ceiling lighting.

2.4.5 Hydrochloric Acid Experiments

A control experiment in which hydrochloric acid was substituted for phosphoric acid was designed to establish whether the phosphoric acid contributed to the SA degradation and the subsequent formation of the by-products. The solution consisted of 20 mg/L SA, 0.067 M potassium phosphate and sufficient hydrochloric acid to reduce the pH of the suspension to 3.0.

2.4.6 Hydrochloric acid and *t*-BuOH Experiments

An additional set of experiments involving a solution of 20mg/L SA, 0.067 M potassium phosphate, hydrochloric acid and 0.01 M tertiary butyl alcohol were also performed to investigate the role of hydroxyl radicals on the degradation of SA and subsequent formation of by-products.

2.4.7 Low Ozone - Setting 1 - SA Only Experiments (SAO)

Lastly, a set of experiments were performed at the lowest possible ozone generator setting without any potassium phosphate buffering solution or phosphoric acid.

The study consisted of multiple experiments using a SA mixture, each of which was 4 hours in duration. Water samples were spiked by adding 20 mg/L of SA. The pH of the solution was reduced to approximately 3.0 with the addition of the salicylic acid. The final volume of each solution was 1.5 L. Six types of solutions/suspensions were tested in the experiments, as noted in Table 2.2. The control solution contained 20 mg/L SA solution in DDI water with no potassium phosphate or phosphoric acid. SAO stands for salicylic acid only. The inlet gaseous oxygen pressure was set to 55 kPa and the ozone generator was set to 1 on a scale of 1-10 with ten being the highest voltage.

Table 2.2: Six Types of SAO Experimental Solutions

Experiment Type	Solution Components	Short Form
1	CS + pure O_2	SAO Control
2	CS + 4 mg/L O_3 gas	SAO O_3
3	CS + 10 mg/L O_3 gas	SAO 10 mg/L Fe_2O_3
4	CS + 100 mg/L Fe_2O_3 + O_2	SAO 100 mg/L Fe_2O_3
5	CS + 10 mg/L Fe_2O_3 + O_3	SAO 10 mg/L Fe_2O_3 + O_3
6	CS + 100 mg/L Fe_2O_3 + O_3	SAO 100 mg/L Fe_2O_3 + O_3

**CS = Control Solution*

Chapter 3

Iron Oxide Nanoparticle Results

3.1 Surface Area Calculations

The approximate surface area for the iron oxide nanoparticles were given by the manufacturer (NanoAmor, Texas, USA) as 50 m^2/g. This is equivalent to 5.0 m^2/L for the 100 mg/L solutions and 0.5 m^2/L for the 10 mg/L solutions. The approximate filtering area available from the iron oxide-coated ceramic membrane filtration experiments performed by Karnik et al. (2009) for a 5 kD membrane ranged from 4.45 - 5.17 m^2/g.

3.2 Adsorption Results

Adsorption experiments were performed with 10, 20, 40, 60, 80 and 100 mg/L Fe_2O_3 at both pH 3 (with phosphoric acid) and pH 8 (with phosphoric acid and sodium hydroxide) with no noticeable SA degradation observed and no by-products formed, as is shown in Figures B.3 and B.4.

3.3 pH 3 Results

Linear regression analysis was used on calibration curves to determine sample concentrations of SA, 2,3-DHBA and 2,5-DHBA. Calibration curves were prepared by analysing known concentrations of SA, 2,3-DHBA and 2,5-DHBA and plotting the concentrations against the resulting area counts after analyses by HPLC. Errors in the concentrations interpolated from the regression line were calculated according to the following formulas (Miller and Miller, 1993):

$$s_{y/x} = \left(\frac{\sum_i (y_i - \hat{y}_i)^2}{n-2}\right)^{1/2} \tag{3.1}$$

(Equation 5.6 in Miller and Miller, 1993)

$$s_{x_o} = \frac{s_{y/x}}{b}\left(\frac{1}{m} + \frac{1}{n} + \frac{(y_o - \bar{y})^2}{b^2 \sum_i (x_i - \bar{x})^2}\right)^{1/2} \tag{3.2}$$

(Equation 5.10 in Miller and Miller, 1993)

A 95% confidence limit was used for the corresponding error calculations. The statistic $S_{y/x}$ given by Equation 3.1 gives the deviations of the y-data about predicted values. $\hat{y}_i$ are the predicted y-values at a given concentration and the y_i values are the measured area counts. S_{x_0}, calculated according to equation 3.2, represents the estimated standard deviation of x_0, which is the estimated concentration based on the equation of the regression line. The x_i values are the known concentrations and $\bar{x}$ represents the average of the known concentrations. $\bar{y}$ represents the average of the measured calibration area counts and y_0 represents the sample area counts for the unknown concentrations. Refer to Appendix A for sample calculations.

3.3.1 High Ozone Experiments - Setting 3

The results for experiments performed at both the high and low ozone generator settings with SA, potassium phosphate (0.067 M) and phosphoric acid (0.001 M) at pH 3 are given in Figures B.5 to B.9. An additional experiment in which no oxygen or ozone was bubbled through the reactor is also presented in these figures.

As may be seen from Figure B.5, SA was found to degrade much more rapidly for those experiments performed at the higher ozone settings. At the high ozone dosage SA was completely degraded within 30 minutes, whereas at the low ozone dosage SA did not completely degrade until about 120 minutes. The experiments without ozone show constant pollutant concentrations with no noticeable degradation occurring.

For the ozonation experiments the concentrations of the by-products generally reached a peak value and then decreased. The formation of 2,3-DHBA was found to be much greater for the experiments performed at a lower ozone setting, as is shown in Figure B.6. At the high ozone dosage, the concentration of 2,3-DHBA reached a maximum value of 1.9 μM, while at the low ozone dosage, maximum concentrations of greater than 4.1 μM were obtained. It should be noted that even in experiments performed without ozone, the formation of 2,3-DHBA was observed. Experiments performed with oxygen in place of ozone resulted in the formation of by-products at concentrations between 0.5 and 0.9 μM, which evolved after 60 minutes. An experiment performed without oxygen or ozone, resulted in maximum 2,3-DHBA concentrations of 2.4 μM, which was greater than that observed with the high ozone

setting experiments.

Similar to that observed with 2,3-DHBA, ozonation resulted in the formation of 2,5-DHBA, the concentration of which reached a maximum value within 30 min and then decreased. Concentrations of 2,5-DHBA were found to be approximately the same for experiments performed at both high and low ozone settings, although at the lower ozone setting, the maximum value was slightly less, as is shown in Figure B.7. With the high ozone setting experiments, the concentration of 2,5-DHBA reached a maximum value of 3.6 μM, while at the low ozone setting the concentration peaked at 3.1 μM. 2,5-DHBA formation was also observed during experiments performed without ozone. Experiments carried out with oxygen in place of ozone resulted in by-product concentrations between 0.3 and 0.8 μM which evolved after 60 minutes. An experiment performed without oxygen or ozone, resulted in even greater 2,5-DHBA concentrations than that observed in the oxygen experiments, reaching a maximum concentration of 1.8 μM.

Aqueous ozone levels were shown to reach peak concentrations and then decline to a steady-state value. Figure B.8 reveals the shift of the peak with time at lower ozone settings. Maximum concentrations between 300 and 380 μM were observed 120 minutes into the experiment for the lower ozone setting experiments, while concentrations between 225 and 270 μM were found to occur 30 minutes into the experiment for the high ozone setting experiments. The concentrations shown in Figure B.8 are averaged values from triplicate aqueous ozone samples. Error bars shown represent the 95% confidence intervals.

The inlet gaseous ozone levels for the high ozone experiments ranged from 225 to 275 μM during the course of the experiments, as may be seen in Figure B.9. The corresponding outlet gaseous ozone levels steadily climbed to 150 - 200 μM and then reached a plateau. The inlet gaseous ozone levels for the lower ozone setting experiments reveal that the experiments were performed at a much lower gaseous ozone concentration of approximately 80 μM. The outlet low ozone concentrations are relatively consistent, varying at most by 25 μM.

3.3.2 Long-Term Experiment

The results of an 8 hour experiment performed at the high ozone setting with 100 mg/L Fe_2O_3, SA, potassium phosphate (0.0067 M) and phosphoric acid (0.001 M) at pH 3 are presented in Figures B.10 and B.11. The 4 hour experimental results from the same set of experiments are also presented as a means of comparison.

It is evident from Figure B.10 that the aqueous ozone concentrations ap-

pear to reach steady state concentrations ranging from 15 to 40 μM after 2 hours at the high ozone setting. These results confirm that four hours should be sufficient time for the aqueous ozone concentrations to reach steady-state levels over the course of an experiment.

The gaseous inlet and outlet ozone concentrations achieved after 240 minutes remained fairly constant over the course of the next 4 hours, as is shown in Figure B.11.

3.3.3 Dark Experiment

Results for experiments performed with SA, potassium phosphate (0.067 M) and phosphoric acid (0.001 M) at pH 3 are given in Figures B.12 and B.13. By-product formation was still observed when the experiment was carried out in the absence of light, ruling out the possibility of photo-oxidation.

The results for a control experiment performed in the dark, presented in Figure B.12, indicate that 2,3-DHBA evolved in a similar concentration range as was observed from experiments performed in the presence of fluorescent lighting. Figure B.13 shows similar findings for 2,5-DHBA.

3.3.4 Hydrochloric acid experiments

Results for experiments performed with SA, potassium phosphate, phosphoric acid or hydrochloric acid and, in some cases, t-BuOH at pH 3 are given in Figures B.14, B.15, B.16.

Although in the control experiment (pH 3, with 0.01 M hydrochloric acid and 0.01 M t-BuOH) the initial SA concentration was greater than the oxygen control solutions, it is obvious from Figure B.14 that the SA was not degraded to any noticeable extent. In the presence of 0.01 M hydrochloric acid (no t-BuOH), however, there appears to be a 6.7% loss of SA over the 4 hour period. The observed decrease in SA concentration is statistically significant at the 95% level according to a two-tailed t-test.

The concentration of 2,3-DHBA formed during the control experiment performed with hydrochloric acid (0.01 M) in place of phosphoric acid (0.001 M) reached greater levels than were observed during the high ozone experiments. The results shown in Figure B.15 depict increasing by-product concentrations over the first 30 minutes of the experiment. The concentration then levels off to approximately 2.7 μM

for the duration of the experiment, results that are comparable to by-product levels noted during previous experiments performed at pH 3 with 0.001 M phosphoric acid. It is very important to note that when *t*-BuOH was added to the same hydrochloric acid control solution no measurable amount of 2,3-DHBA was formed.

The concentration of 2,5-DHBA was also quite high for the control experiment performed with hydrochloric acid in place of phosphoric acid. The results shown in Figure B.16 illustrate rising by-product concentrations over the first 30 minutes of the experiment. The concentration reached approximately 1.7 μM before levelling out, which is also comparable to by-product levels noted during previous experiments performed with the buffering solution at pH 3 with phosphoric acid. The addition of *t*-BuOH to the same hydrochloric acid control solution resulted in no measurable amount of 2,5-DHBA being formed as well.

3.3.5 Low Ozone Experiments - Setting 1 - No Buffer (potassium phosphate)

The results for experiments performed with SA only at pH 3 are given in Figures B.17 to B.21.

The SA concentrations observed for pH 3 solutions without potassium phosphate and at a lower ozone setting took longer to completely degrade than when subjected to the high ozone setting, as may be seen from Figure B.17. The ozonation experiment results all agree with each other very well, indicating that SA was not degraded any faster when in the presence of iron oxide. The experiments conducted with oxygen instead of ozone show no statistically relevant degradation.

The concentrations of 2,3-DHBA peaked after approximately 15-30 min of ozonation at 2.5 - 4.9 μM. Figure B.18 shows decreasing by-product concentrations following the peak values with complete disappearance of the compound by 240 minutes. These results are comparable to the studies conducted at pH 3 on solutions containing 0.67 M potassium phosphate available in Figure B.6. The experiments conducted without ozone all showed no by-product formation.

2,5-DHBA peak concentrations were much higher than 2,3-DHBA, ranging from 6.8 - 9.6 μM. Figure B.19 shows similar decreasing by-product concentrations following the peak values with complete disappearance of the compound also occurring by 240 minutes. Results shown in Figure B.7 for the studies conducted at pH 3 on solutions containing potassium phosphate (0.067 M) show much lower peak concentrations for the low ozone experiments, the maximum of which was 3.6 μM. The experiments conducted without ozone also all show no by-product formation.

The maximum aqueous ozone concentrations for the experiments conducted at the lower ozone setting in the absence of potassium phosphate were much lower than that observed for the low ozone experiments in suspensions containing 0.067 M potassium phosphate. Figure B.20 shows that maximum aqueous ozone levels of 160 - 225 μM occurred between 120 and 180 minutes, whereas peak aqueous ozone concentrations of 300 - 380 μM are shown in Figure B.8 at the low ozone setting in the presence of potassium phosphate.

Figure B.21 shows that experiments carried out at the lower ozone generator setting were indeed subjected to lower gaseous ozone levels with inlet concentrations of approximately 100 μM and outlet concentrations hovering around 50 μM. Experiments performed at the high ozone setting showed inlet gaseous ozone concentrations ranging from 225 - 270 μM with observed outlet concentrations of 150 - 200 μM.

3.4 pH 8 Results

Results for experiments performed with SA, potassium phosphate (0.067 M) and phosphoric acid (0.001 M) at pH 8 are given in Figures B.22 to B.26.

The SA was degraded much more rapidly at pH 8 than that observed at pH 3 for the same high ozone levels and solution/suspension composition. Figure B.22 displays SA degradation curves for ozonation experiments which reveal that there was no noticeable difference in SA concentrations with and without iron oxide nanoparticles. The SA concentrations appear to remain constant during oxygen experiments with no measurable degradation.

Maximum 2,3-DHBA concentrations of approximately 8.2 μM were recorded for the high pH experiments, as is shown in Figure B.23. With high ozone dosages, at pH 3, the maximum 2,3-DHBA concentration was 1.9 μM as is seen in Figure B.6. The lower pH results showed by-product formation occurred during the oxygen experiments, yet there was no measurable 2,3-DHBA formed during the oxygen tests at pH 8.

2,5-DHBA was formed in even greater concentrations than was 2,3-DHBA at high pH and high ozone dosages, the results of which are given in Figure B.24. Peak concentrations of 16.2 - 19.5 μM were observed, which are six times as large as peak concentrations recorded at pH 3. Although by-product formation occurred during the pH 3 oxygen experiments, no measurable 2,5-DHBA formed during the oxygen tests at pH 8.

As can be seen from Figure B.25, aqueous ozone concentrations reached a maximum of 75 - 85 μM before decreasing to steady state levels of approximately 30 μM. These peak concentrations are much lower than the 225 - 270 μM aqueous ozone levels observed for the high ozone generator setting, pH 3 experiments with potassium phosphate shown in Figure B.8.

As shown in Figure B.26, the inlet gaseous ozone levels ranged from 250 - 300 μM during the first hour of the experiments but then became relatively constant at approximately 270 μM. The outlet gaseous ozone levels steadily climbed to 170 - 200 μM then reached a plateau around 180 - 200 μM. These results are comparable with the gaseous ozone levels observed during the pH 3 experiments at the high ozone setting with potassium phosphate available in Figure B.9.

3.4.1 Low Ozone Experiments - Setting 1- No Buffer (potassium phosphate)

The results for experiments performed with SA, phosphoric acid and sodium hydroxide at pH 8 are given in Figures B.27 to B.31.

The SA degradation curves for low ozonation experiments presented in Figure B.27 show that the rate of SA degradation was much slower than when solutions containing potassium phosphate were subjected to high ozonation levels. The pH 8 experiments show that SA is almost completely degraded after 60 minutes, whereas the pH 3 tests conducted on the same solutions show slower degradation with complete disappearance of the study compound by 120 minutes. It is also apparent from Figure B.27 that the ozone experiment with no iron oxide actually resulted in more rapid SA degradation than the ozone tests with iron oxide, showing that in this case iron oxide is not catalyzing the decomposition of SA.

The formation of 2,3-DHBA in solutions/suspensions without potassium phosphate are shown in Figure B.28. Peak concentrations of 10.0 - 10.4 μM were observed for the low ozone setting experiments without potassium phosphate, which is slightly higher than the 8.2 μM peak observed for the high ozone experiments with potassium phosphate. The 2,3-DHBA concentrations reached a maximum at 15 minutes for the low ozone experiments without potassium phosphate, whereas the peak was found to occur at 5 minutes for the high ozone experiments with potassium phosphate. The results for the low ozone experiments at pH 8 without potassium phosphate also show higher 2,3-DHBA concentrations than that observed in the low ozone experiments without potassium phosphate at pH 3, which reached maximum levels of 4.9 μM.

The formation of 2,5-DHBA in solutions/suspensions without potassium phosphate are shown in Figure B.29. Peak concentrations of 20.1 - 24.0 μM were observed for the low ozone setting experiments at pH 8 without potassium phosphate, which is slightly higher than the 19.5 μM maximum observed for the high ozone experiments at pH 8 with potassium phosphate. The 2,5-DHBA concentrations reached a maximum between 15 to 20 minutes into the experiment for the low ozone experiments at pH 8 without potassium phosphate, whereas the peak was found to occur at 10 minutes for the high ozone, pH 8 experiments with potassium phosphate. The findings for the low ozone experiments at pH 8 without potassium phosphate also show higher 2,5-DHBA concentrations than the low ozone experiments at pH 3 without potassium phosphate, which reached maximum levels of 9.6 μM.

The aqueous ozone levels for the ozone only experiments showed higher peak concentrations than the experiments performed with iron oxide, as may be seen in Figure B.30. The observed aqueous ozone peaks were not due to fluctuations in the inlet and outlet gaseous ozone concentrations, which showed similar concentrations for experiments performed with iron oxide to those observed for the ozone only experiments. Gaseous inlet and outlet concentrations are depicted in Figure B.31.

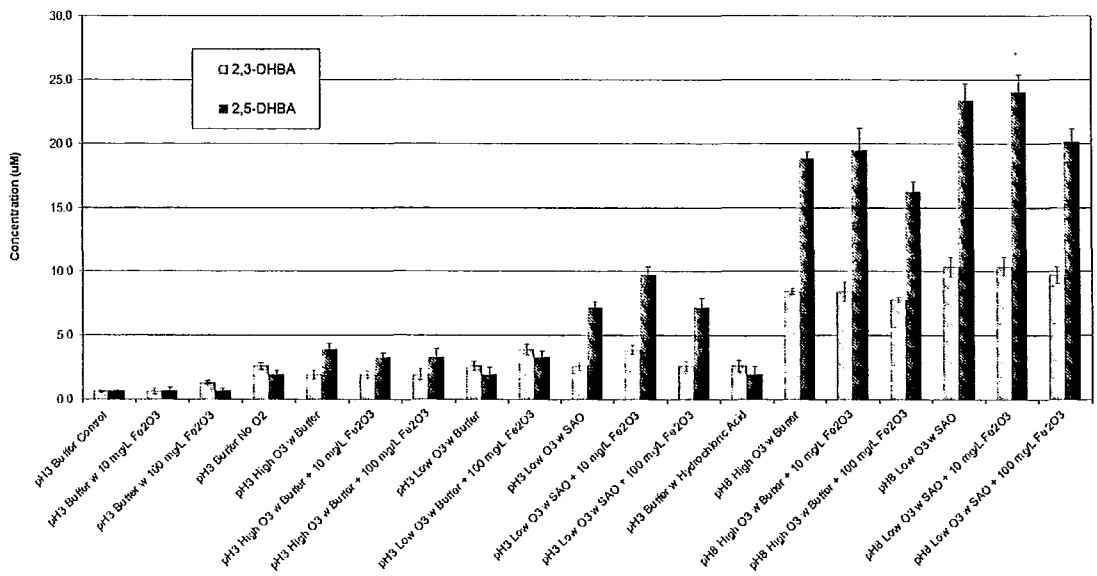

Figure 3.1: Maximum Observed By-Product Concentrations
Full-size: Appendix I, Page 35, Figure B.32

The maximum by-product formation results are summarized in graphical format in Figure 3.1. It is obvious from the figure that 2,5-DHBA generally was formed in greater concentrations than was 2,3-DHBA. By-products were formed in

the highest quantities at pH 8 when compared to pH 3 as is shown in Figure B.33. Figure B.34 illustrates the variation in by-product formation for experiments conducted without ozone and without aeration. The presence of by-products without oxygen or ozone bubbled through the suspensions led to more investigations to find the hydroxyl radical source. The grouping of experiments with ozone at the high and low pH serve as an excellent point of reference for the non-ozonated experiments, including the HCLA experiments. The differences between experiments performed with and without the potassium phoshpate buffer may be seen in Figure B.35. This figure clearly shows that by-product formation was considerably higher when experiments were conducted in the absence of the pH buffer, regardless of pH. The potassium phosphate is therefore having an effect on the by-product formation.

3.5 Kinetics

The rate constants for the degradation of SA were obtained by creating a semi-log plot of SA concentration (μM) vs. time (minutes), an example of which is shown in Figure 3.2.

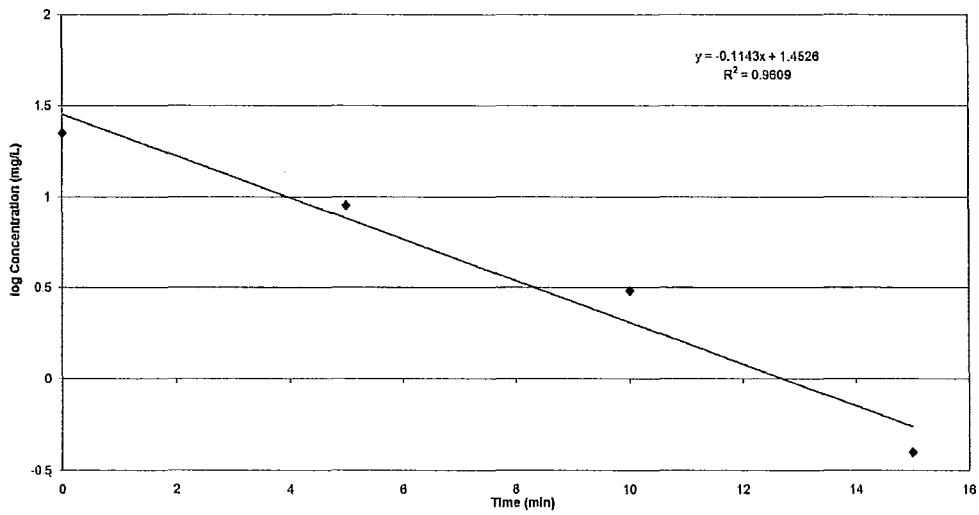

Figure 3.2: Semilog Plot of SA Concentration with Time at pH 8 with Potassium Phosphate, 10 mg/L Fe_2O_3 at the High Ozone Setting
Full-size: Appendix I, Page 37, Figure B.36

Table 3.1 summarizes the SA degradation rate constants for all of the ozonated experiments. The results clearly show that SA was degraded much more

rapidly during experiments conducted at pH 8 with potassium phosphate buffering agent at the high ozone setting than during any other studies. Experiments carried out at the low ozone setting with phosphate buffer at pH 3 were performed only once and therefore do not have an associated standard deviation for the degradation rate constant. These results do show, however, that the presence of the buffering agent has no noticeable effect on SA degradation rates when compared with the rate constants determined at pH 3 in the absence of potassium phosphate at the low ozone setting. The ozone only experiments performed at pH 3 at the high ozone setting and at pH 8 at the high ozone setting both show that SA was degraded more rapidly than in the presence of Fe_2O_3. The experiments performed at the low ozone setting have rate constants that are within standard deviation range of each other for their respective pH conditions. It is also evident from Table 3.1 that experiments performed at the low ozone setting carried out at pH 8 degraded SA more rapidly.

Table 3.1: Six Types of Experimental Solutions

Experiment	Average K (min^{-1})	Standard Deviation	Average R Sq.
pH3 High O_3 w Buffer	-0.0502	0.0039	0.9890
pH3 High O_3 w Buffer + 10 mg/L Fe_2O_3	-0.0407	0.0047	0.9886
pH3 High O_3 w Buffer + 100 mg/L Fe_2O_3	-0.0507	0.0034	0.9873
pH3 Low O_3 w Buffer	-0.0154	N/A	0.9831
pH3 Low O_3 w Buffer + 100 mg/L Fe_2O_3	-0.0139	N/A	0.9845
pH3 Low O_3 w SAO	-0.0149	0.0007	0.9864
pH3 Low O_3 w SAO + 10 mg/L Fe_2O_3	-0.0141	0.0008	0.9921
pH3 Low O_3 w SAO + 100 mg/L Fe_2O_3	-0.0134	0.0002	0.9842
pH8 High O_3 w Buffer	-0.1301	0.0037	0.9638
pH8 High O_3 w Buffer + 10 mg/L Fe_2O_3	-0.1173	0.0030	0.9561
pH8 High O_3 w Buffer + 100 mg/L Fe_2O_3	-0.0910	0.0027	0.9770
pH8 Low O_3 w SAO	-0.0330	0.0045	0.9892
pH8 Low O_3 w SAO + 10 mg/L Fe_2O_3	-0.0293	0.0022	0.9894
pH8 Low O_3 w SAO + 100 mg/L Fe_2O_3	-0.0280	0.0025	0.9915

Chapter 4

Discussion

In an attempt to explain the observed formation of by-products during experiments without ozone, experiments were conducted in the dark and with the addition of the hydroxyl radical scavenger, *t*-BuOH. Figures B.12 and B.13 show that by-product formation was still observed when the experiments were carried out in the dark, thereby eliminating the possibility of a photo-oxidation mechanism. Studies at pH 3 on SA solutions with hydrochloric acid (0.01 M) in place of phosphoric acid (0.001 M) as well as with potassium phosphate (0.067 M) showed significant by-product formation, as demonstrated in Figures B.15 and B.16. The by-product formation with the hydrochloric acid solution was comparable to that observed for the pH 3 phosphoric acid solution at the high ozone dosage with the exception that the non-ozonated studies showed no subsequent by-product disappearance. SA is known to react with $^{\bullet}OH$ to produce the by-products 2,3 and 2,5-DHBA, so $^{\bullet}OH$ must be produced in the system in the absence of ozone. Experiments performed with 0.001 M *t*-BuOH ($^{\bullet}OH$ scavenger) still showed some by-product formation. With the addition of 0.01 M *t*-BuOH no measurable amount of by-product formation was observed, thus verifying that in the absence of ozone the reaction involves a radical pathway.

The fritted glass bubbler was coated with a layer of iron oxide nanoparticles due to the repeated suspension experiments. A complex iron system was therefore present during all of the experiments, including the studies in which no additional iron oxide was added, such as the hydrochloric acid, phosphoric acid and the ozone only experiments. The formation of by-products 2,3-DHBA and 2,5-DHBA during pH 3 potassium phosphate experiments without ozone can be explained by the presence of iron in the system due to the bubbler. It is possible that SA is capable of reducing surface Fe(III) groups to Fe(II), enabling Fe(II) to detach from the oxide surface more easily than Fe(III) (Valverde et al. 1976). The Fe(II) in the solution/suspension could then be oxidized by oxygen to Fe(III), which in turn oxidizes the SA to produce 2,3-DHBA and 2,5-DHBA. The Fe(III) would therefore be reduced to Fe(II), resulting in a cyclic oxidation/reduction reaction mechanism. The lack of by-product

formation during the first 15 minutes of the hydrochloric acid and phosphoric acid control experiments is effectively explained by the time required for sufficient Fe(II) to accumulate for the reaction to proceed at a measureable rate.

The absence of by-product formation during control experiments without potassium phosphate at both pH 3 and pH 8 indicates that the buffering solution also plays a role in the reductive dissolution of the iron oxide and subsequent oxidation of SA. Sulzberger et al. (1989) show how phosphate can form binuclear inner-sphere surface complexes with iron oxide, thus allowing the surface Fe(III) to be more efficiently reduced.

The lack of by-products formed for the same phosphoric acid control experiments with potassium phosphate at pH 8 could be explained by the greater degree of adsorption of Fe(II) on hematite (α-Fe_2O_3) above pH 5 (Mulvaney et al. 1988), which would reduce the rate of dissolution of the iron oxide (LaLind & Stone 1989). Fe(III) could also be detached in acid solutions by the adsorption of H+ (Sulzberger et al. 1989).

Although iron oxide coatings were shown to catalyze the degradation of SA in the ozonated ceramic membrane experiments conducted by Karnik et al. (2007), none of the experiments showed enhanced SA degradation rates with the addition of iron oxide, regardless of Fe_2O_3 concentration (surface area), pH or the addition of the potassium phosphate buffer. Table 3.1 shows that while most experiments resulted in SA degradation rates that were within standard deviation of each other, the rate constants obtained during high ozone dosage experiments at pH 8 with the potassium phosphate buffer solution showed steadily decreasing rate constants with increasing Fe_2O_3 loadings. Hydroxyl radicals may have been scavenged by the iron oxide surface-bound phosphate, which led to decreasing levels of SA degradation.

Figure B.32 shows that the by-products 2,3-DHBA and 2,5-DHBA were formed in higher concentrations at pH 8 than at pH 3 for all experiment configurations. This can be attributed to the increased hydroxide ion concentrations present at higher pH values, which have been shown to promote ozone decomposition (Hoign and Bader 1976). The faster ozone decomposition leads to the generation of more hydroxyl and other radical species that are capable of oxidizing SA to produce the observed by-products. Increased by-product levels were also observed during experiments conducted at the low ozone setting when compared with the high ozone setting results. Although SA was shown to be degraded more rapidly at the higher ozone setting, the resulting by-products were also more rapidly oxidized during the higher ozone setting experiments, resulting in lower observed 2,3-DHBA and 2,5-DHBA formation peak concentrations.

The presence of potassium phosphate also affected ozone concentrations, as may be seen in Figure B.10. Experiments conducted at the high gaseous ozone setting were shown to have relatively constant inlet and outlet gaseous ozone concentrations, which was also true of experiments carried out at the lower gaseous ozone setting. The gaseous ozone concentrations were therefore unaffected by the presence of potassium phosphate or changes in pH. The peak aqueous ozone concentration was, however, affected with the observed peak almost doubling if phosphate was present at pH 3 for the low ozone dosage experiments. It is postulated that the hydroxyl scavenging ability of phosphate, which has been noted by several researchers (Bower & Miller 2002, Andreozzi et al. 1998a, Masten et al. 1996), is repsonsible for the decreased ozone decomposition rates, which in turn led to higher aqueous ozone concentrations. Much lower peak aqueous ozone concentrations were also observed during the pH 8 experiments compared with the pH 3 experiments. This result is logical, given that more alkaline solutions contain more hydroxide ions which promote the rapid decomposition of ozone, as was previously stated (Hoign and Bader 1976). Despite the variations in peak aqueous ozone concentrations, the final ozone concentrations for all experiments were relatively the same at approximately 1.5 mg/L.

Increased aqueous ozone levels observed during ozonation experiments in the absence of iron oxide (refer to Figure B.30) suggest that Fe2O3 catalyzes the decomposition of ozone. Hydroxyl radicals may be scavenged in the process, resulting in the observed decreased SA degradation rates for experiments performed with Fe2O3 nanoparticles.

Further studies investigating the amounts of Fe(III), Fe(II), $^{\bullet}OH$ and the role of potassium phosphate are recommended to verify the proposed iron oxide reduction mechanism. Experiments exploring the adsorption of phosphate would also be useful, as SA was shown not to adsorb to the Fe_2O_3 nanoparticles and exhibited no degradation except in the presence of potassium phosphate buffer. Similar experiments examining the possible effects of TiO_2 nanoparticles on the degradation of SA with ozone would also be desirable to discern the role of the ceramic membrane support used in the experiments of Karnik et al.(2007).

Chapter 5

Conclusions

5.1 Conclusions

A comparison of SA degradation rates revealed that, in most cases, the addition of iron oxide nanoparticles had no statistical effect. Only during experiments at pH 8 with potassium phosphate at the high ozone dosage were SA degradation rates shown to decrease with increasing iron oxide concentrations. The addition of 100 mg/L Fe_2O_3 resulted in even slower SA degradation rates than were observed with the addition of 10 mg/L of Fe_2O_3 nanoparticles, likely due to the hydroxyl radical scavenging ability of the iron oxide for the catalytic decomposition of ozone.

The use of a phosphate buffer at pH 3.0 resulted in noticeable contaminant degradation, which contradicts observations by Andreozzi et al. (1998b) during his work on manganese oxide and pyruvic acid. It appears as though the potassium phosphate buffer also scavenged hydroxyl radicals during the ozonation experiments, resulting in reduced ozone decomposition rates. The presence of potassium phosphate in the system also resulted in measureable by-product formation at pH 3, suggesting that the buffer also contributed to by-product formation. The effect of phosphate buffers is therefore not very well understood as there is little documentation of these effects in the literature.

It was proposed that by-product formation was observed during oxygenated experiments due to the presence of a complex iron system with phosphate. The importance of $^{\bullet}OH$ formation was highlighted through experiments conducted with 0.01 M *t*-BuOH, a hydroxyl radical scavenger, which resulted in no measurable by-product formation or SA degradation. Experiments performed in the dark resulted in the same by-product formation, eliminating the possibility of a photo-catalytic mechanism. The mechanism of iron oxide reduction has never before been shown in the literature to be dependent upon the formation of hydroxyl radicals in a photo-independent system.

5.2 Summary

The importance of the proposed iron oxide reduction mechanism in the absence of a photo-oxidation dependent system should not be overlooked. Most groundwater systems are not exposed to light and come into contact with iron and iron oxides on a regular basis. This mechanism shows how it might be possible for metals to become reduced in groundwater systems and migrate as suspended or dissolved particles, effectively changing the water chemistry. Mobilized iron particles would be capable of reacting with a wide variety of compounds, participating in redox reactions and changing the redox potential of groundwater systems. This in turn could lead to adsorbed trace metals, such as arsenic, cobalt, zinc and nickel being released into the water column due to the mobilization of the iron. The oxidation of Fe(II) to Fe(III) can affect other redox systems as well, and was shown to increase the pyritic oxidation rate by Welch et al. (2000) resulting in the release of trace metals into the water column. The proposed mechanism allows for the redox reaction to take place in deep aquifers through abiotic mechanisms. The dissolution of iron oxides affects the cycle of iron, both in the ocean as well as fresh water systems.

Previous researchers have studied the dissolution of iron oxides by reductants in thermal and photochemical processes, but have never examined the possible effect of hydroxyl radicals on the dissolution characteristics. The newly proposed mechanism demonstrates the transformation of iron in natural water systems, the presence of which could alter water groundwater chemistry and change modelling scenarios. For example, arsenic is a common contaminant in groundwater, which has been shown to be effectively adsorbed to natural iron ore composed primarily of hematite (Zhang et al., 2004). How would the adsorption of arsenic be affected by the dissolution of the iron oxide into the groundwater? The adsorption of arsenic to iron is one of the most common remediation stategies for groundwater systems and the effectiveness of this technique could be jeopardized if the complex iron system leads to the desorption of arsenic back into the water column. Arsenic removal has become a priority in some artificially recharged aquifers due to the dissolution of arsenic through changing water chemistry (Bell et al., 2009). The presence of phosphate was also shown to decrease the adsorption of arsenic in experiments conducted by Zhang et al. (2004). The effects of phosphate on such a complex system surely deserve further investigation.

Ground water modelers are constantly trying to predict where as well as how fast contaminant plumes (concentrated areas of pollutants within a water system) are moving. The reductive dissolution of iron oxide could significantly affect the amount of contaminants that are able to be mobilized. The possibility of contaminants

playing an active role in their own oxidation/reduction with the complex iron system means that by-product formation could take place in environments in which sufficient degradation conditions were thought not to exist.

5.3 Recommendations for Further Work

The newly proposed mechanism of iron oxide reduction should be verified through additional investigations. Characterization of the iron oxide nanoparticles, in particular the amount of Fe(III) and Fe(II) present in the system under various conditions, would help to illuminate how the redox reactions proceed. Field studies to evaluate the possibility of this mechanism occurring in the natural environment could also serve as an effective means of verification. Contaminants of concern which are known to interact with iron and iron oxides, such as arsenic, should be carefully evaluated to ensure that harmful substances are not re-entering the water columns after remediation of contaminated water columns. Studies focusing on the concentrations of hydroxyl radicals being generated in the absence of ozone would be beneficial to track scavenging substances. The role of potassium phosphate in the system and its affect on the iron oxide reduction mechanism are areas of study that are important due to the widespread use of this common pH buffer. In this set of experiments, only the iron oxide coating from ceramic membrane-ozonation experiments conducted by Karnik et al. (2005a, 2005b, 2007, 2009) was tested in the system. The ceramic membrane support material, titanium dioxide (TiO_2), should also be tested in the system to evaluate the effect of the membrane support on by-product formation.

References

Albarran, G., & Schuler, R. (2003). Concerted effects in the reaction of OH radicals with aromatics: Radiolytic oxidation of salicylic acid. *Radiation Physics and Chemistry*, 67, 279-285.

Allemane, H., Delouane, B., Paillard, H., & Legube, B. (1993). Comparative efficiency of three systems (O3/O3-H2O2 and O3/TiO2) for the oxidation of natural organic matter in water. *Ozone Science and Engineering*, 15, 419.

American Water Works Association. (1993). Brominated DBPs [editorial]. *Journal of American Water Works Association*, 41.

Andreozzi, R., Caprio, V., Ermellino, I., Insola, A., & Tufano, V. (1996). Ozone solubility in phosphate-buffered aqueous solutions: Effect of temperature, tert-butyl alcohol and pH. *Industrial and Engineering Chemistry Research*, 35, 1467-1471.

Andreozzi, R., Caprio, V., Insola, A., Marotta, R., & Tufano, V. (1998a). The ozonation of pyruvic acid in aqueous solutions catalyzed by suspended and dissolved manganese. *Water Resources*, 32 (5), 1492-1496.

Andreozzi, R., Insola, A., Caprio, V., Marotta, R., & Tufano, V. (1998b). The use of manganese dioxide as a heterogeneous catalyst for oxalic acid ozonation in aqueous solution. *Applied Catalysis A*, 32 (5), 1492-1496.

Avramescu, S., Mihalache, N., Bradu, C., Neata, M., & Udrea, I. (2009). Catalytic ozonation of acid red 88 from aqueous solutions. *Catalysis Letters*, 129, 273-280.

Bader, H., & Hoigne, J. (1981). Determination of ozone in water by the indigo method. *Water Research*, 15, 449-456. *APHA Standard Methods*, 20th ed., 4-144-4-146, Method 4500-O3 B (1998).

Bell, K., Wiseman, L., & Turner, L. (2009). Designing pretreatment to control arsenic leaching in ASR facilities. *American Water Works Association*, 101, 6, 74 - 84.

Bower, K., & Miller, C. (2002). Filter sand - phosphate buffer effect on 2,4-dinitrotoluene ozonation. *Journal of Environmental Engineering*, 128 (2), 131-136.

Devulapelli, V.G., & Sahle-Demessie, E. (2008). Catalytic oxidation of dimethyl sulfide with ozone: Effects of promoter and physico-chemical properties of metal oxide catalysts. *Applied Catalysis A: General*, 348, 86-93.

Einaga, H., & Ogata, A. (2009). Benzene oxidation with ozone over supported manganese oxide catalysts: Effect of catalyst support and reaction conditions. *Journal of Hazardous Materials*, 164 (2-3), 1236-1241.

Gunten, U.v., & Hoign, J. (1994). Bromate formation during ozonation of bromide-containing waters: Interaction of ozone and hydroxyl radical reactions. *Environmental Science and Technology*, 28, 1234-1242.

Hart, E.J., Sehested, K., & Holcman, J. (1983). Molar absorptivities of ultraviolet and visible bands of ozone in aqueous solutions. *Analytical Chemistry*, 55, 46-49.

Hoign, J., & Bader, H. (1976). The role of hydroxyl radical reactions in ozonation processes in aqueous solutions. *Water Research*, 10, 377-386.

Joseph, Y., Ranke, W., & Weiss, W. (2000). Water on FeO(111) and Fe3O4(111): Adsorption behaviour on different surface terminations. *Journal of Physical Chemistry B*, 104, 3224-3236.

Karnik, B., Davies, S., Baumann, M., & Masten, S. (2005a). The effects of combined ozonation and filtration on disinfection by-product formation. *Water Research*, 39, 2839-2850.

Karnik, B., Davies, S., Chen, K., Jaglowski, D., Baumann, M., & Masten, S. (2005b). Effects of ozonation on permeate flux of nanocrystalline ceramic membranes. *Water Research*, 39, 728-734.

Karnik, B., Davies, S., Baumann, M., & Masten, S. (2007). Use of salicylic acid as a model contaminant to investigate hydroxyl radical reaction in an ozonation-membrane filtration hybrid process. *Environmental Engineering Science*, 24(6), 852-860.

Karnik, B., Baumann, M., Corneal, L.M., Masten, S. & Davies, S. (2009). TEM characterization of iron-oxide-coated ceramic membranes. *Journal of Material*

Science, 44, 4148-4154.

LaLind, J.S. & Stone, A.T. (1989). Reductive dissolution of goethite by phenolic reductants. *Geochimica et Cosmochimica Acta*, 53 (5), 961-971.

Lartiges, S.B, & Garrigues, P.P. (1995). Degradation kinetics of organophosphorous and organonitrogen pesticides in different waters under various environmental conditions. *Environmental Science and Technology*, 29, 1246-1254.

Legube, B., & Leitner, N. (1999). Catalytic ozonation: A promising advanced oxidation technology for water treatment. *Catalysis Today*, 53, 61-72.

Leitner, N. Karpel Vel, Delouane, B., Legube, B. and Luck, F. (1999). Effects of catalysts during ozonation of salicylic acid, peptides and humic substances in aqueous solution. *Ozone: Science & Engineering*, 21(3), 261-276.

Li, Y.Q. (2000). Potassium phosphate as a catalyst for the Knoevenagel condensation. *Journal of Chemical Research (S)*, 524-525.

Jen, J.F., Leu, M.F., & Yang, T.C. (1998). Determination of hydroxyl radicals in an advanced oxidation process with salicylic acid trapping and liquid chromatography. *Journal of Chromatography A*, 796, 283-288.

Lin, S. & Gurol, M. (1998). Catalytic decomposition of hydrogen peroxide on iron oxide: Kinetics, mechanism and implications. *Environmental Science and Technology*, 32, 1417-1423.

Lin, Y.C., & Lin, C.H. (2008). Catalytic and photocatalytic degradation of ozone via utilization of controllable nano-Ag modified on TiO2. *Environmental Progress*, 27 (4), 496-502.

Logager, T., Holcman, J., Sehested, K., & Pedersen, T. (1992). Oxidation of ferrous ions by ozone in acidic solutions. *Inorganic Chemistry*, 31, 3523-3529.

Mackenzie, D.L., & Masten, S.J. (2004). *Principles of Environmental Engineering and Science.* New York, McGraw-Hill Companies Inc. p. 357.

Masten, S.J., Shu, M., Galbraith, M.J., & Davies, S.H.R. (1996). Oxidation of chlorinated benzenes using advanced oxidation processes. *Hazardous Waste and Hazardous Materials*, 13 (2), 265-282.

Metcalf & Eddy Inc., November (2003). *Wastewater Engineering Treatment and*

Reuse, Fourth Edition. McGraw-Hill Companies Inc., 1104 - 1131.

Miller, J.C., & Milller, J.N. (1993). *Statistics for Analytical Chemistry, 3rd Edition.* New York, Ellis Horwood Limited.

Mitchell, M.B., Sheinker, & V.N., Cox, W.W. (2007). Room temperature reaction of ozone and dimethyl methylphosphonate (DMMP) on alumina-supported iron oxide. *Journal of Physical Chemistry C*, 111 (26), 9417-9426.

Mulvaney, P., Cooper, R., Grieser, F., & Meisel, D. (1988). Charge trapping in the reductive dissolution of colloidal suspensions of iron(III) oxides. *Langmuir*, 4, 1206-1211.

Nowell, L.H., Hoign, J. (1988). Interaction of iron (II) and other transition metals with aqueous ozone. *Proceedings of the 8th Ozone World Congress*, IOA, Zurich, Switzerland, E80-E95.

Office of Water, November (2005). *Membrane Filtration Guidance Manual.* United States Environmental Protection Agency, EPA 815-R-06-009.

Paode, R.D., Amy, G.L., Krasner, S.W., Summers, R.S., & Rice, E.W. (1997). Predicting the formation of aldehydes and BOM. *Journal of American Water Works Association*, 86, 6, 79-93.

Pi, Y., Ernst, M., & Schrotter, J.C. (2003). Effect of phosphate buffer upon CuO/Al2O3 and Cu (II) catalyzed ozonation of oxalic acid solution. *Ozone Science and Engineering*, 25, 393-397.

Punchard, N.A., & Kelley, F.J. (1996). *Free radicals: A practical approach.* Oxford, Oxford University Press.

Qafisheh, N., Mukhupadhyay, S., Joshi, A., Sasson, Y., Chuah, G.K., & Jaenickes, S. (2007). Potassium phosphate as a high-performance solid base in phase-transfer-catalyzed alkylation reactions. *Industrial and Engineering Chemistry Research.* 46, 3016-3023.

Song, R., Westerhoff, P., Minear, R., & Amy, G. (1997). Bromate minimization during ozonation. *Journal of American Water Works Association*, 86, 6, 99-78.

Sreethawong, T., & Chavadej, S. (2008). Color removal of distillery wastewater by ozonation in the absence and presence of immobilized iron oxide catalyst. *Journal of Hazardous Materials*, 155 (3), 486-493.

Staehelin, J., & Hoign, J. (1985). Decomposition of ozone in water in the presence of organic solutes acting as promoters and inhibitors of radical chain reactions. *Environmental Science and Technology*, 19(12), 1206-1213.

Sulzberger, B., Suter, C., Siffert, C., Banwart, S., & Strumm, W. (1989). Dissolution of Fe(III)(hydr)oxides in natural waters; Laboratory assessment on the kinetics controlled by surface coordination. *Marine Chemistry*, 28, 127-144.

Valverde, N. & Wagner, C. (1976). Considerations on the kinetics and the mechanism of the dissolution of metal oxides in acidic solutions. Ber. Bunseges. *Physical Chemistry*, 80, 330.

Wang, H.C., Chang, S.H., Hung, P.C., Hwang, J.F., & Chang, M.B. (2007). Catalytic oxidation of gaseous PCDD/Fs with ozone over iron oxide catalysts. *Chemosphere*, 71, 388-397.

Wedley, S., & Waite, T.D. (2004). *Fenton Processes.* S. Parsons (Ed.), Advanced Oxidation Processes for Water and Wastewater Treatment, Cornwall, IWA Publishing, UK, 111-136.

Welch, A., Westjohn, D., Helsel, D., & Wanty, R. (2000). Arsenic in ground water of the United States: Occurrence and geochemistry. *Ground Water*, 38, 4, 589.

Xie, L., & Shang, C. (2006). Effects of copper and palladium on the reduction of bromate by Fe(0). *Chemosphere*, 64, 919-930.

Xing, S., Hu, C., Qu, J., He, H., & Yang, M. (2008). Characterization and reactivity of MnOx supported on mesoporous zirconia for herbicide 2,4-D mineralization with ozone. *Environmental Science and Technology*, 42, 3363-3368.

Yang, L., Hu, C., Nie, Y., & Qu, J. (2009). Catalytic ozonation of selected pharmaceuticals over mesoporous alumina-supported manganese oxide. *Environmental Science and Technology*, 43, 2525-2529.

Zang, W., Singh, P., Paling, E., and Delides, S. (2004). Arsenic removal from contaminated water by natural iron ores. *Minerals Engineering*, 17, 517 - 524.

Appendices

Appendix A

Sample Calculations

A.1 Calibration and Error Calculations

Example taken from June 3, 2009 100 mg/L Fe_2O_3 with ozone at setting 1 and pH 8.

Table A.1: 2,3-DHBA Calibration

Concentration (mg/L)	2,3-DHBA Area Counts
0.005	16396
0.005	28306
0.005	21450
0.025	176721
0.025	185443
0.025	185293
0.05	415275
0.05	405972
0.05	432894
0.25	1793195
0.5	2831328
1.0	6657240

A plot of the data given in Table A.1 with Concentration on the x-axis and Area Counts on the y-axis, called a calibration curve, may be fit in a linear manner defined by the following equation:

$$y = 6469432x + 22945 \tag{A-1}$$

In order to calculate the errors in the concentration obtained through interpolation from the regression line we must first compute the statistic $S_{y/x}$ given by Equation A-2 which gives the deviations of the y-data about predicted values.

$$S_{y/x} = \left(\frac{\sum_i (y_i - \hat{y}_i)^2}{n-2}\right)^{1/2} \quad \text{(A-2)}$$

(Equation 5.6 in Miller and Miller, 1993)

$\hat{y}_i$ are the predicted y-values at a given concentration. For example, at a concentration of 0.005 mg/L the equation of a line with the given data could be represented by:

$$\hat{y} = 6469432(0.005) + 22945 = 55292 \quad \text{(A-3)}$$

The y_i values are the measured area counts, the first of which would be 16396. n is the number of samples, in this case n = 12. Now $S_{y/x}$ can be calculated:

$$s_{y/x} = 158597.9 \quad \text{(A-4)}$$

Next, S_{x_0}, the estimated standard deviation of x_0 can be calculated from Equation A-5:

$$s_{x_0} = \frac{s_{y/x}}{b}\left(\frac{1}{m} + \frac{1}{n} + \frac{(y_o - \bar{y})^2}{b^2 \sum_i (x_i - \bar{x})^2}\right)^{1/2} \quad \text{(A-5)}$$

(Equation 5.10 in Miller and Miller, 1993)

The x_i values are the known concentrations. In this example, $x_i = 0.005$. $\bar{x}$ represents the average of the known concentrations, equal to 0.1658. $\bar{y}$ represents the average of the measured calibration area counts, equal to 1095793. y_0 represents the sample area counts for the unknown concentrations, equal to 0 at time 0 minutes. x_0 represents the estimated 2,3-DHBA concentration based on the equation of the regression line. Equation A-6 shows an example.

$$x_0 = (0 - 22945)/6469432 = -0.004 mg/L \quad \text{(A-6)}$$

The calculated value of x_0 with 0 absorbance results in a very small negative concentration, revealing that there is obviously some error associated with the value. S_{x_0} can now be calculated and is found to equal 0.0164. The error is then 2.57 times S_{x_0} for a 95% confidence interval with N-2 degrees of freedom. The error associated with the estimated concentration is therefore 0.042 mg/L.

A.2 Aqueous Ozone Calculations

At t=0 minutes the measured absorbance is equal to -0.005. The aqueous ozone concentration would then be calculated according to Equation A-7.

$$Concentration(mg/L) = (25 \times |-0.005|)/0.42 = 0.417 mg/L \quad \text{(A-7)}$$

A.3 Gaseous Ozone Calculations

The inlet gaseous ozone absorbance at t=0 was -0.0499, while the absorbance at t=10 minutes was -0.0066. An adjusted absorbance was calculated to 'zero' the absorbance data. The adjusted absorbance at t=0 was calculated according to Equation A-8, while the adjusted absorbance at t=10 was calculated in Equation A-9.

$$adjusted\,absorbance = -0.0499 - 0.0499 = 0 \tag{A-8}$$

$$adjusted\,absorbance = -0.0066 - 0.0499 = -0.0565 \tag{A-9}$$

The gaseous ozone concentration could then be calculated according to Equation A-10, which gives concentrations of 0 mg/L at t=0 and 3.52 mg/L at t=10.

$$Concentration(mg/L) = (47.98 \times 1000 \times |adjusted\,absorbance|)/590 \tag{A-10}$$

Appendix B

Full Size Figures

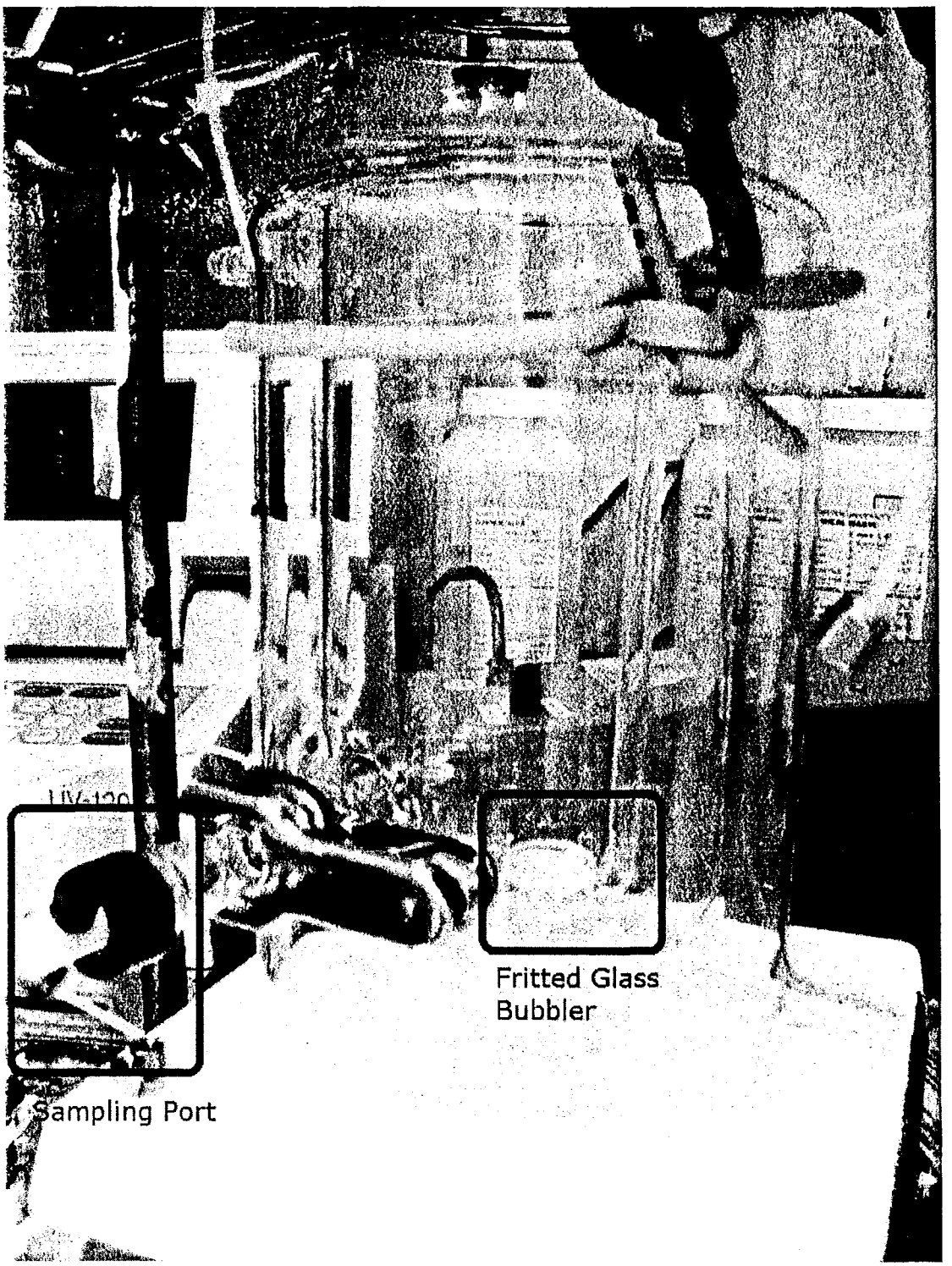

Figure B.1: 1.5 L Glass Reactor Vessel

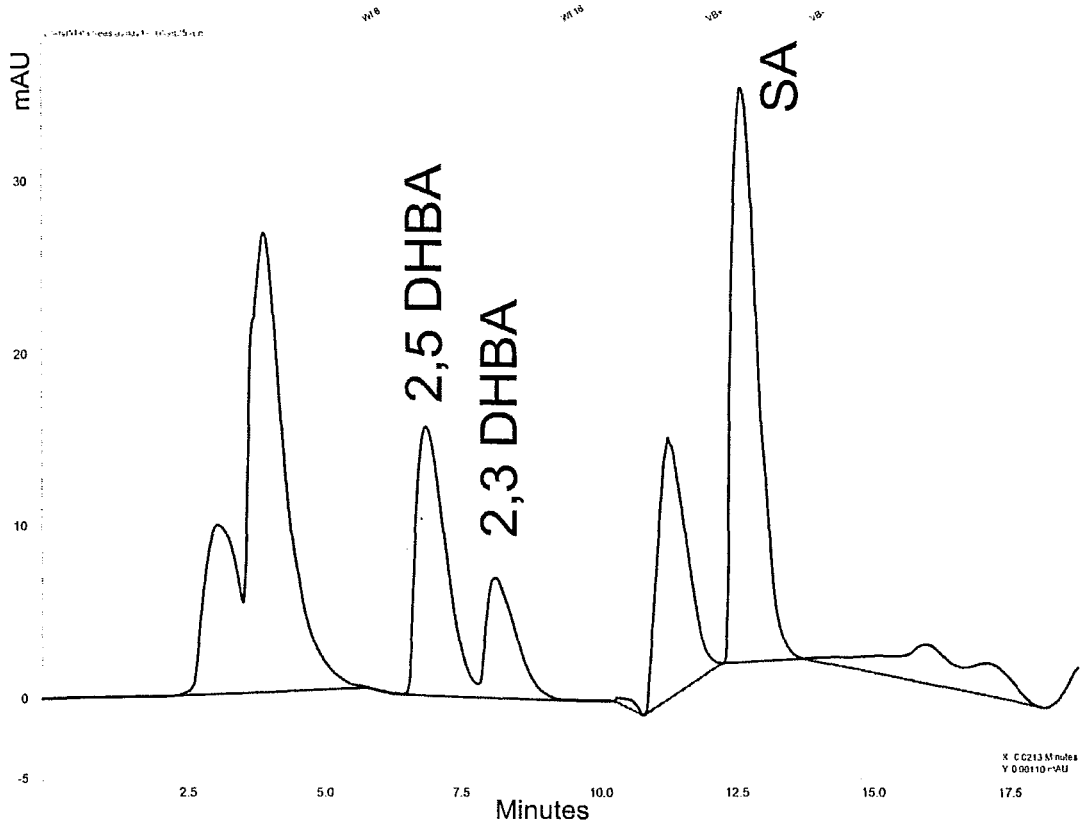

Figure B.2: Sample Chromatogram from May 17, 2009 SAO with Ozone at 25 Minutes

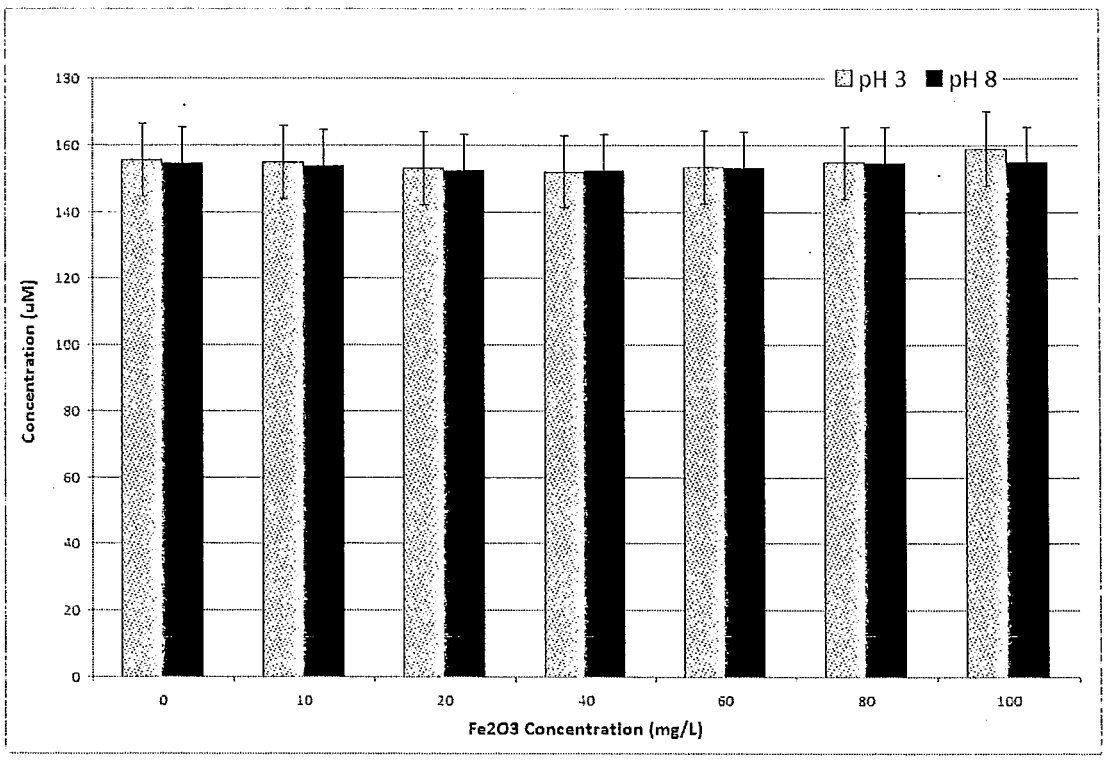

Figure B.3: SA Concentrations for Adsorption Experiments After 1 Hour

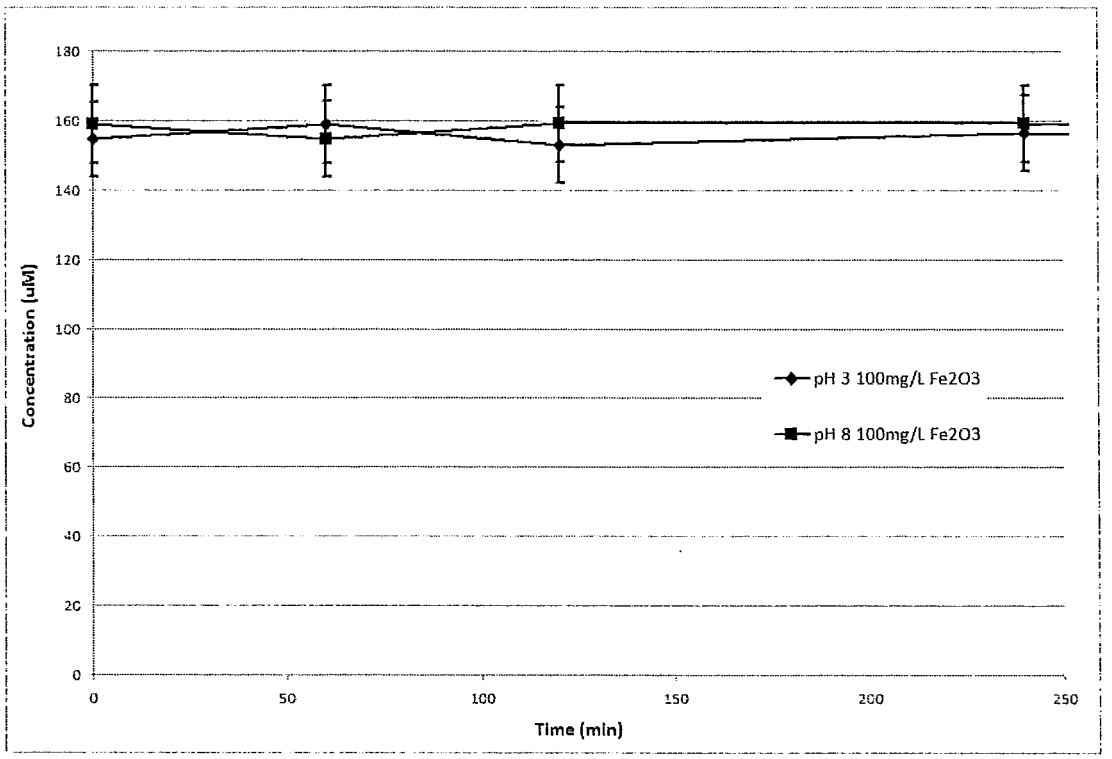

Figure B.4: SA Degradation for 100 mg/L Fe_2O_3 Over 23 Hours

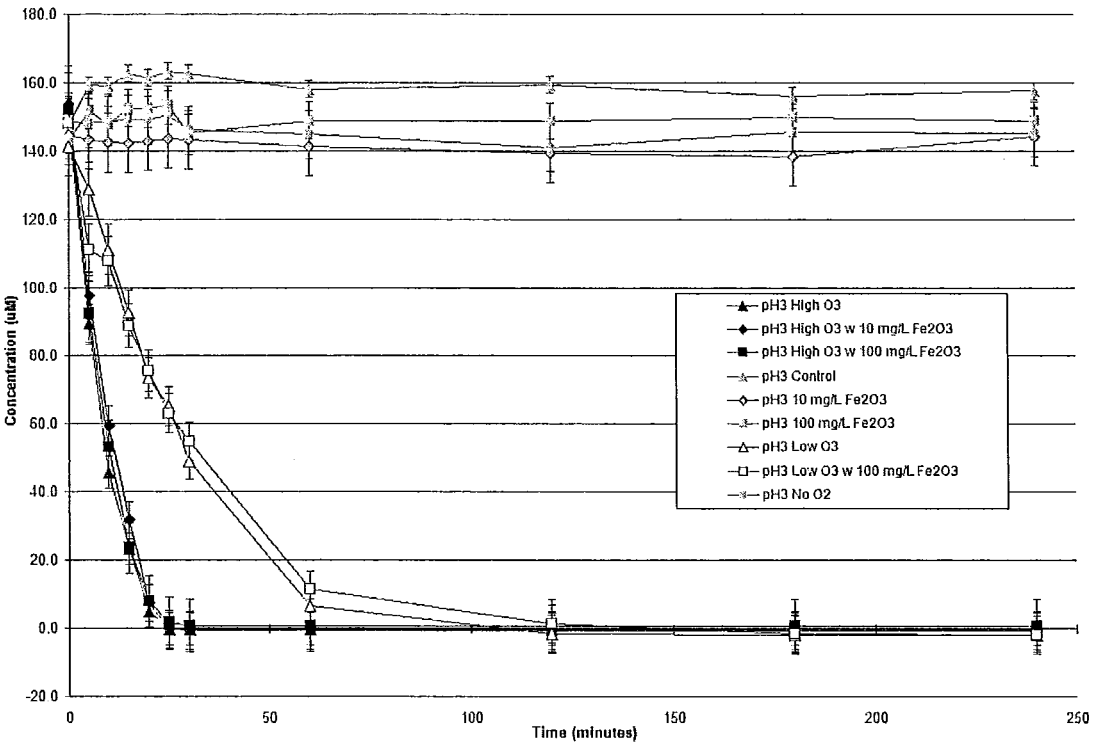

Figure B.5: SA Degradation Curves for Potassium Phosphate Experiments

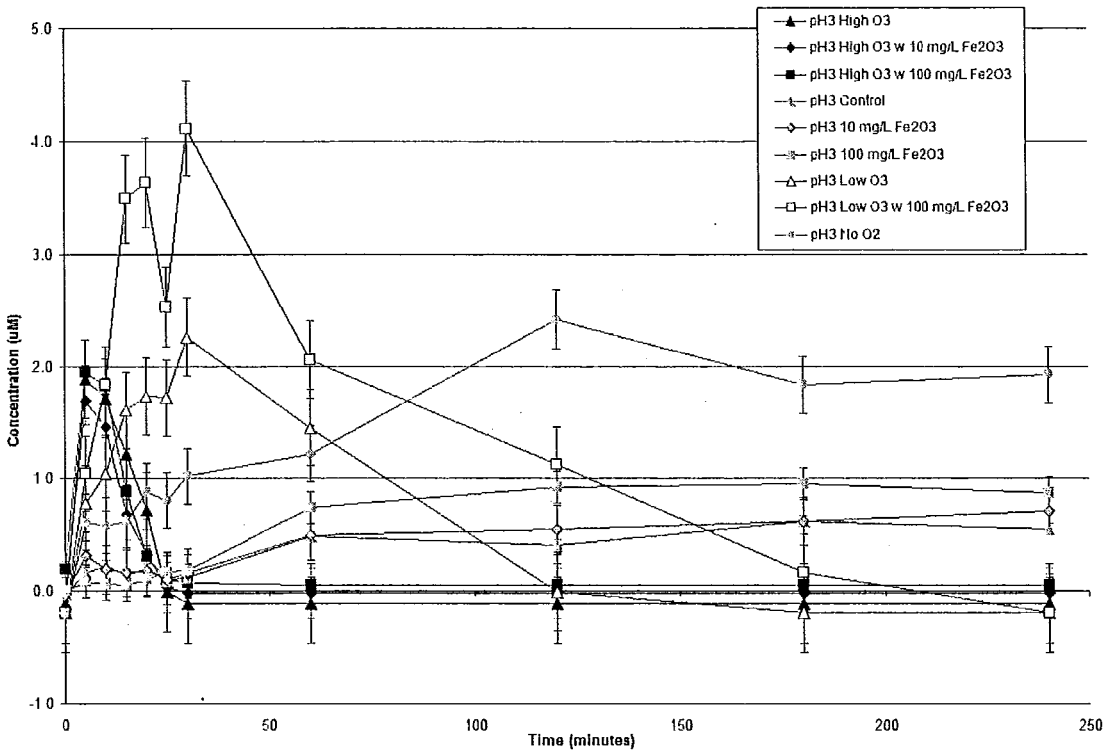

Figure B.6: 2,3-DHBA Formation for Potassium Phosphate Experiments

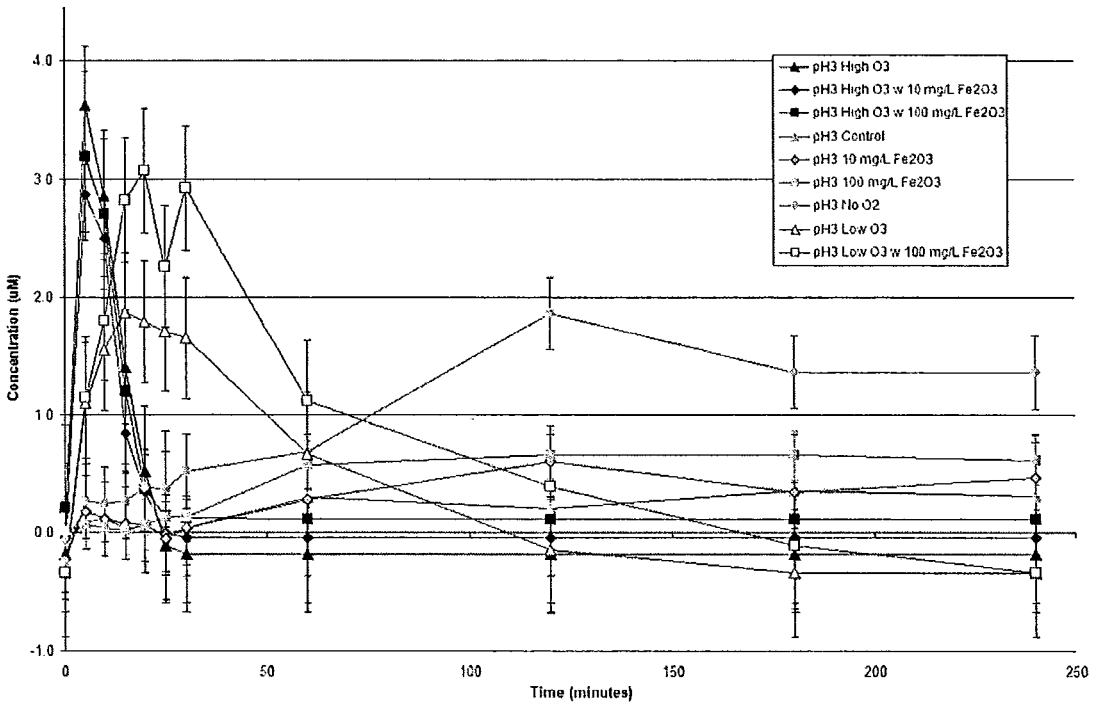

Figure B.7: 2,5-DHBA Formation for Potassium Phosphate Experiments

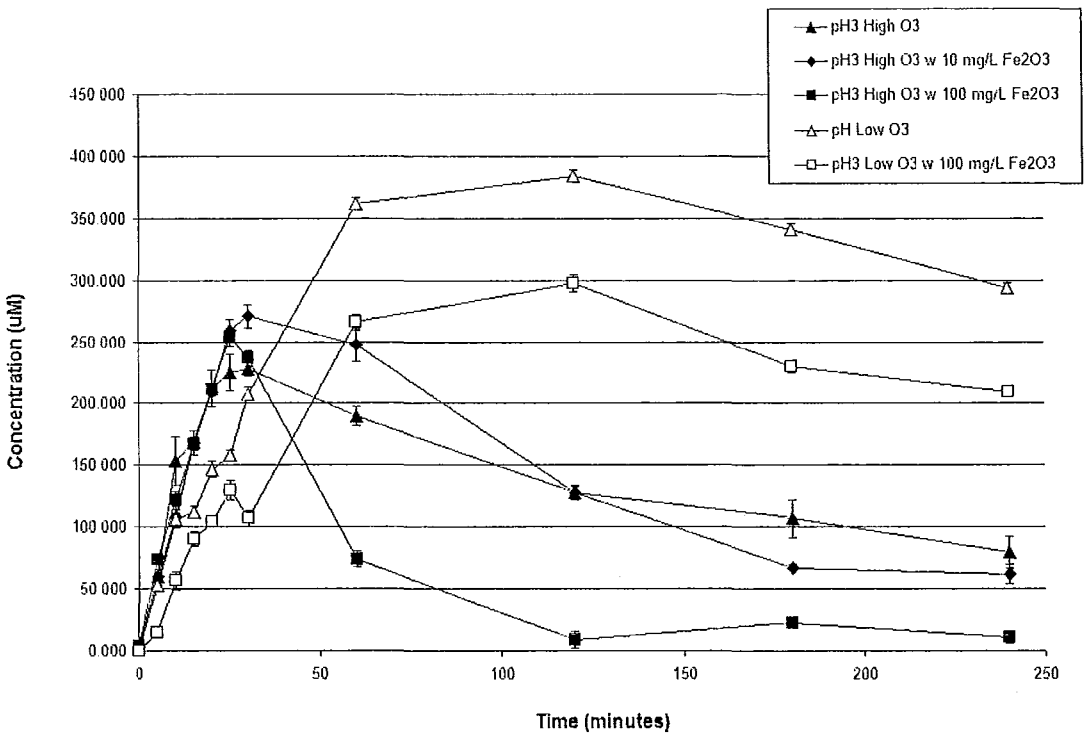

Figure B.8: Aqueous Ozone Levels for Potassium Phosphate Experiments

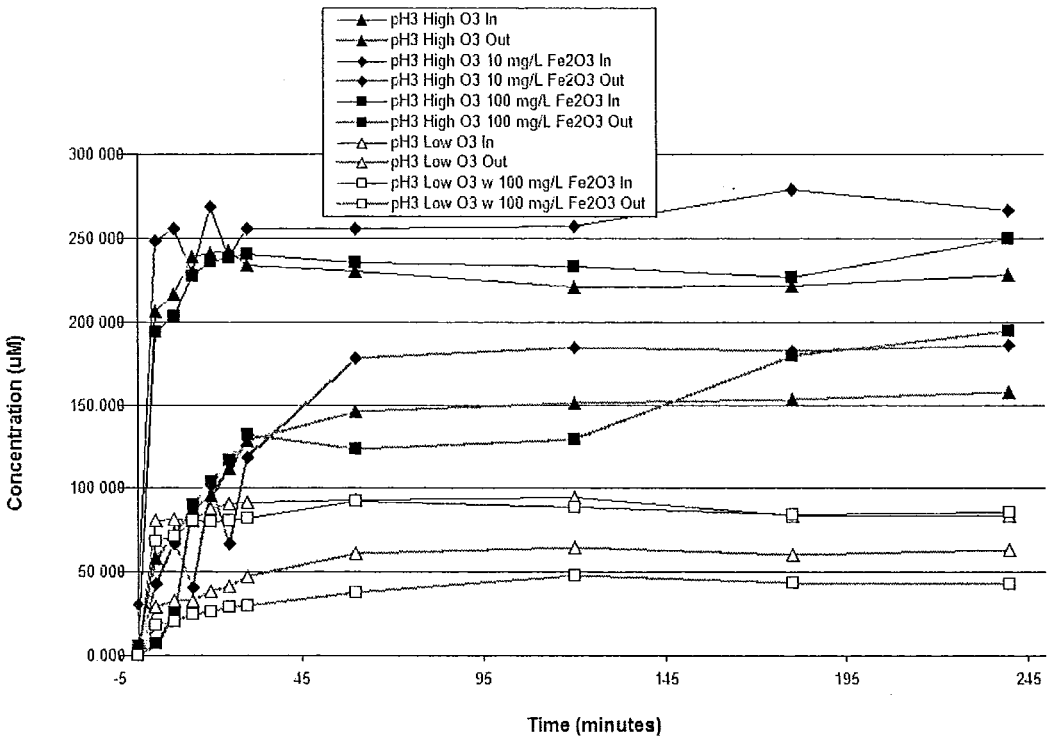

Figure B.9: Gaseous Ozone Levels for Potassium Phosphate Experiments

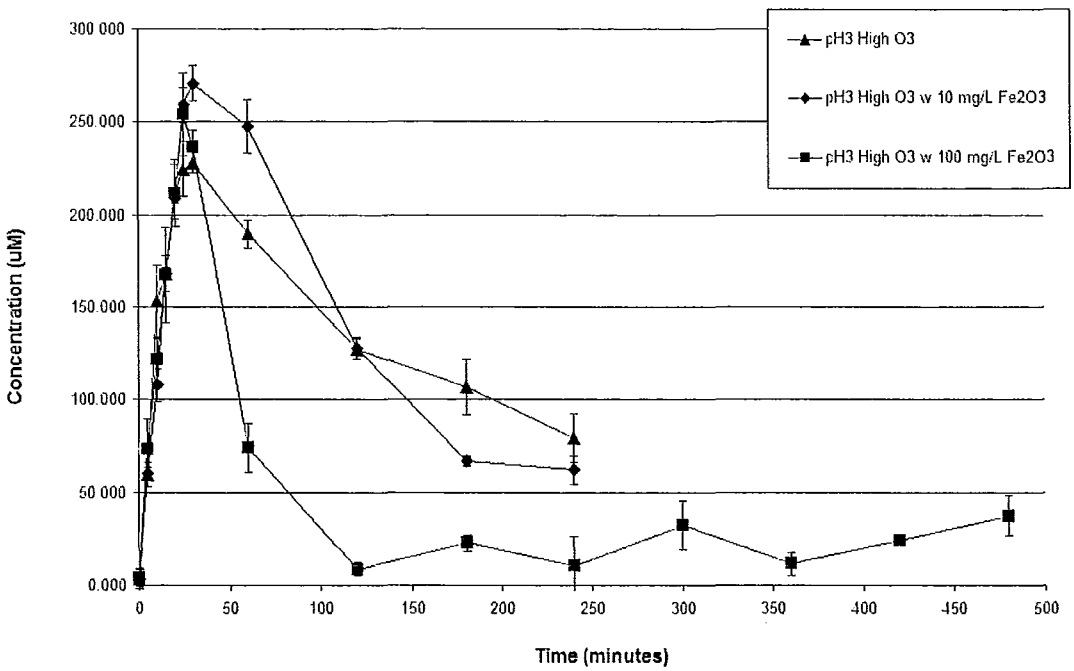

Figure B.10: Aqueous Ozone Levels for Long-term Experiment Comparison

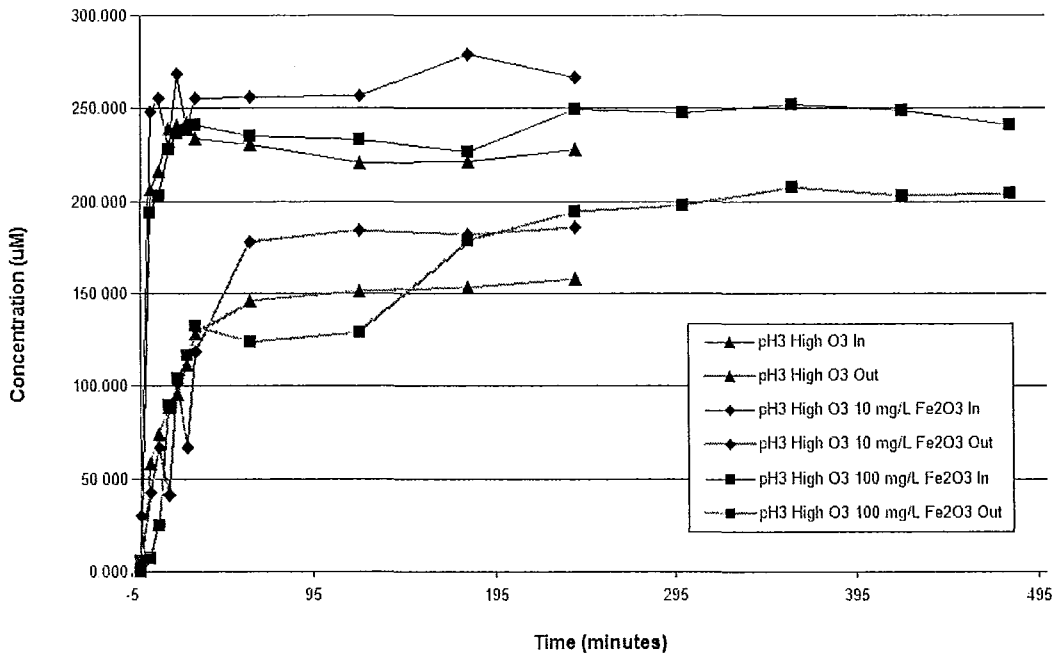

Figure B.11: Gaseous Ozone Levels for Long-term Experiment Comparison

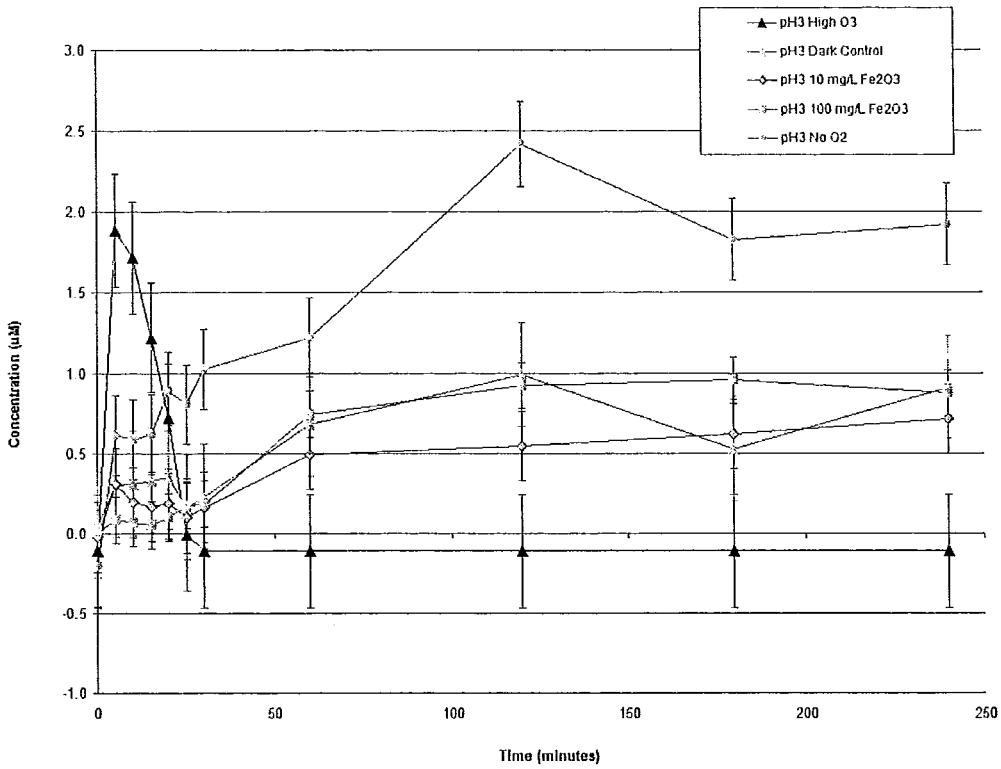

Figure B.12: 2,3-DHBA Formation for Experiments Performed in the Dark

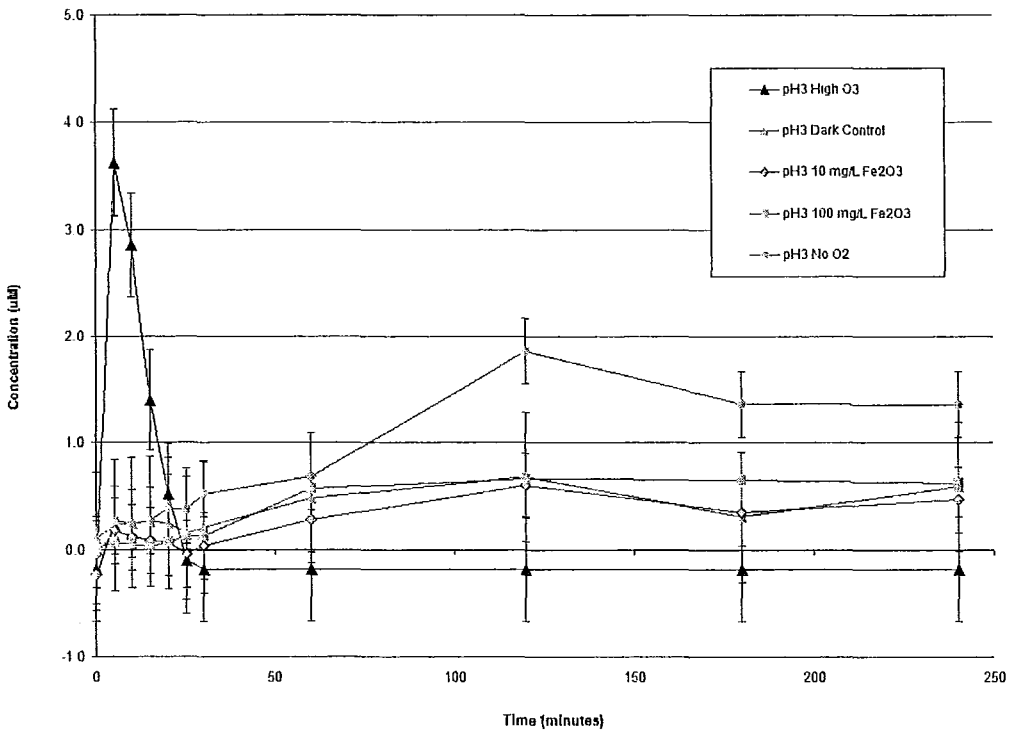

Figure B.13: 2,5-DHBA Formation for Experiments Performed in the Dark

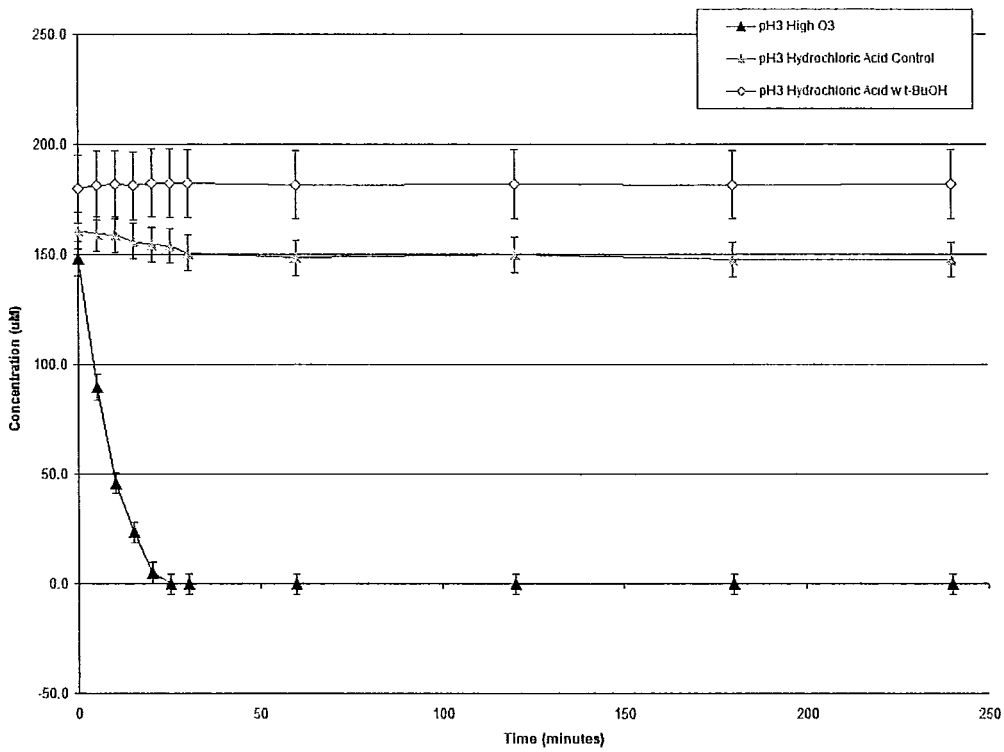

Figure B.14: SA Levels for Experiments with Hydrochloric Acid

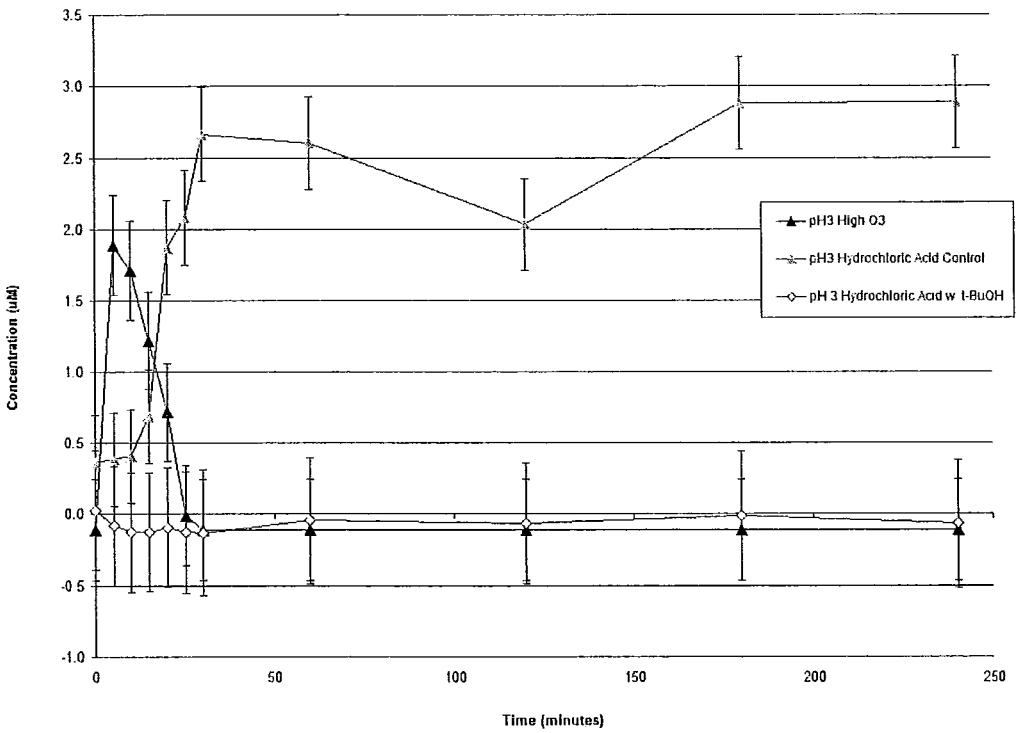

Figure B.15: 2,3-DHBA Formation for Experiments with Hydrochloric Acid

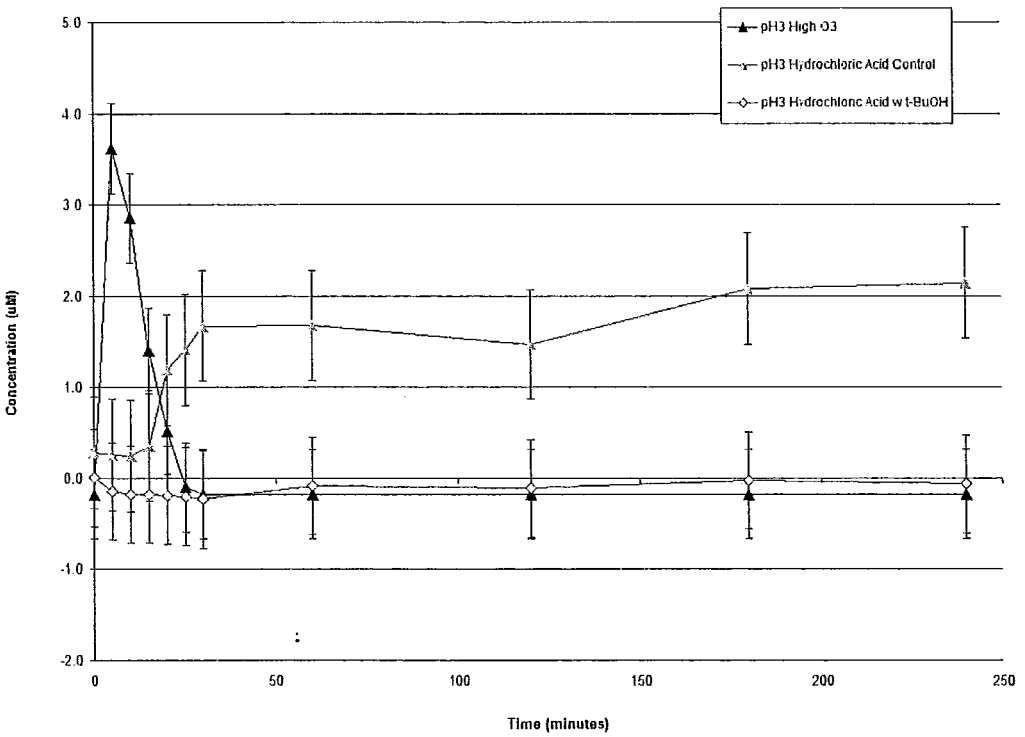

Figure B.16: 2,5-DHBA Formation for Experiments with Hydrochloric Acid

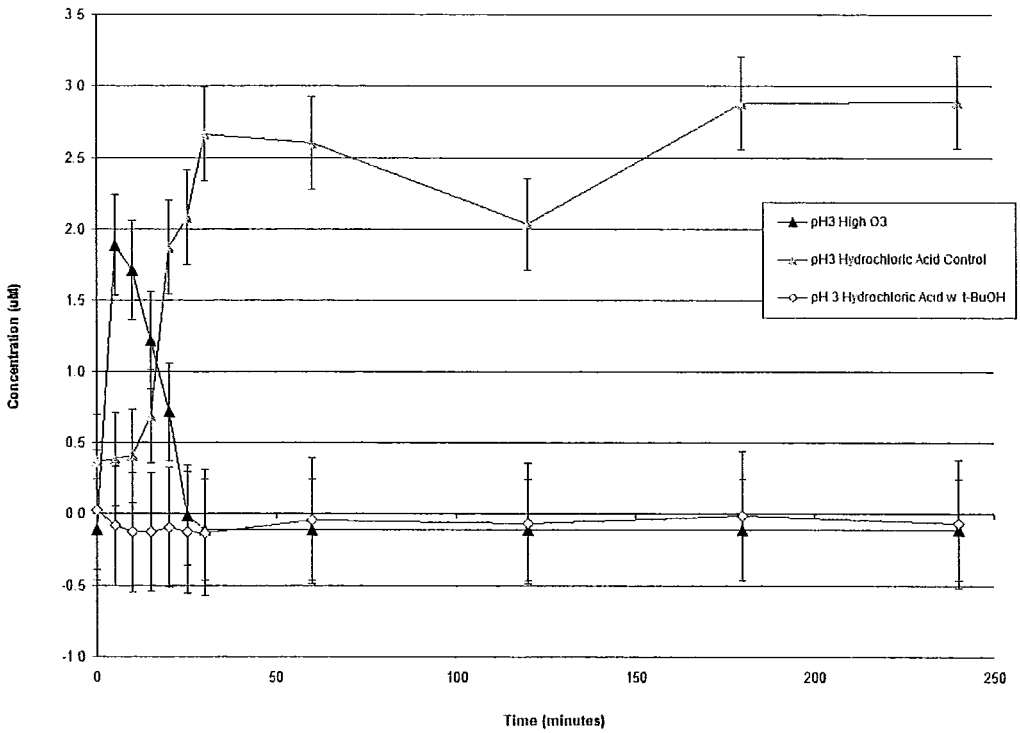

Figure B.17: SA Degradation Curves for SAO Experiments

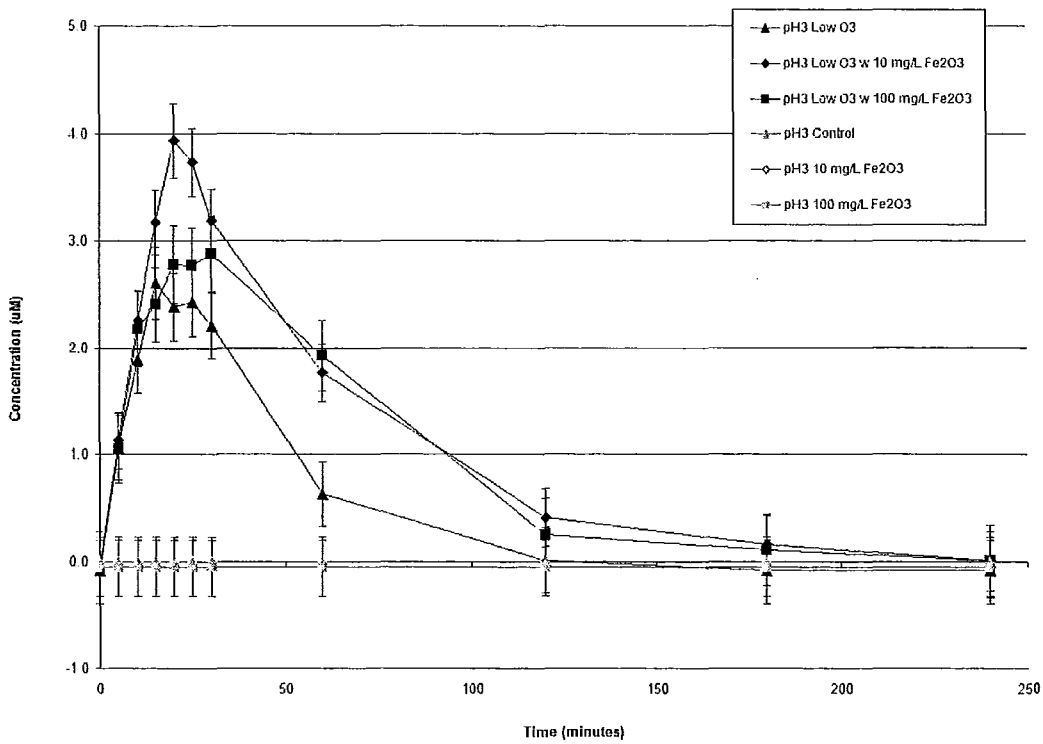

Figure B.18: 2,3-DHBA Formation for SAO Experiments

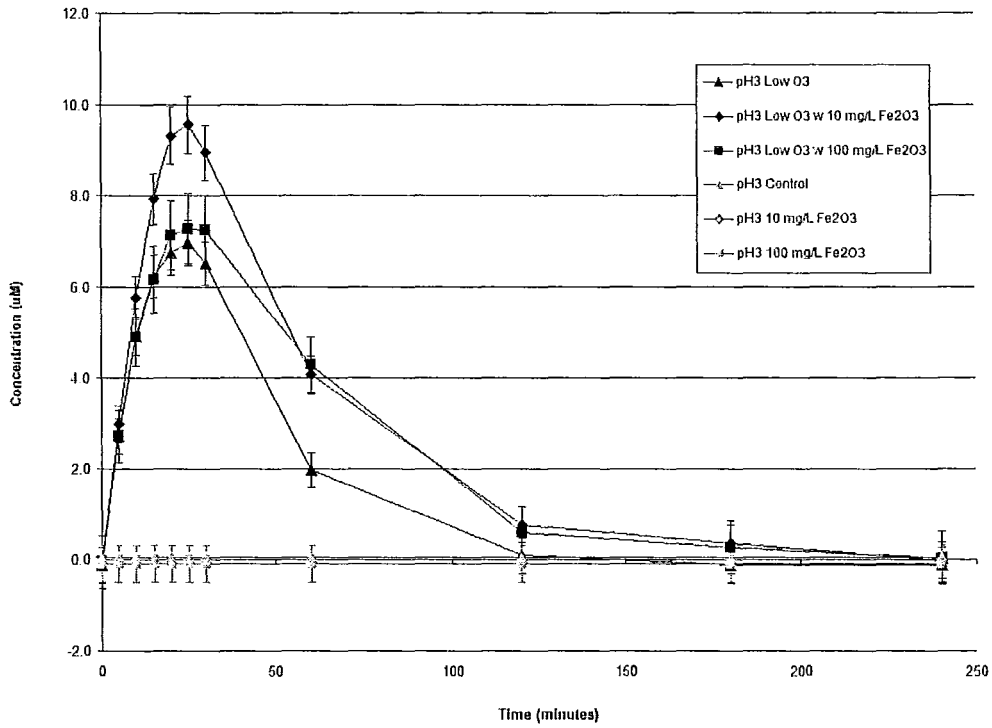

Figure B.19: 2,5-DHBA Formation for SAO Experiments

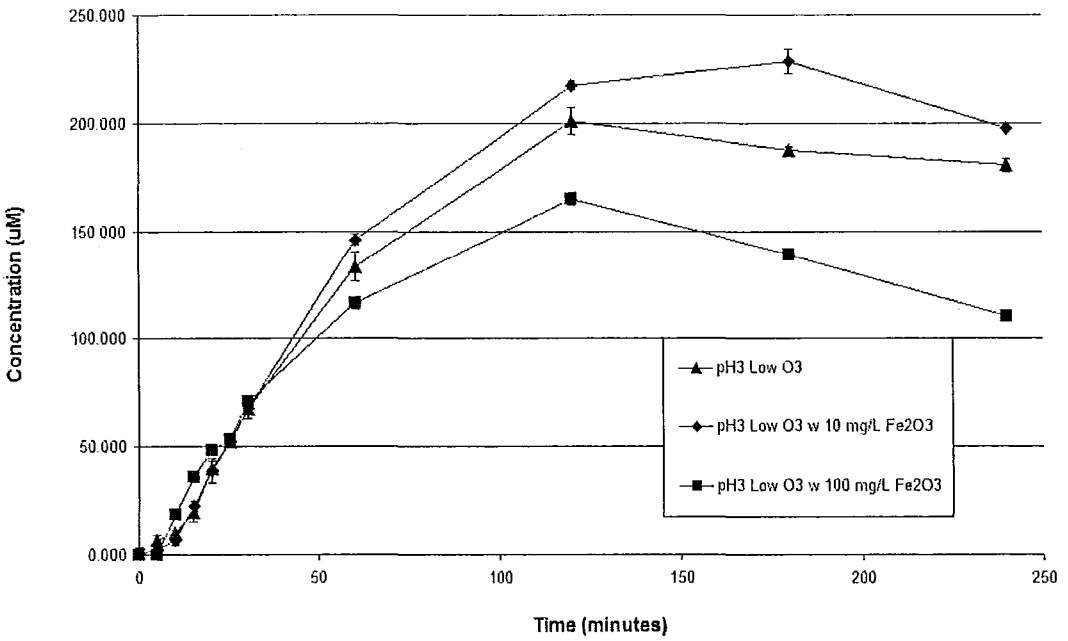

Figure B.20: Aqueous Ozone Levels for SAO Experiments

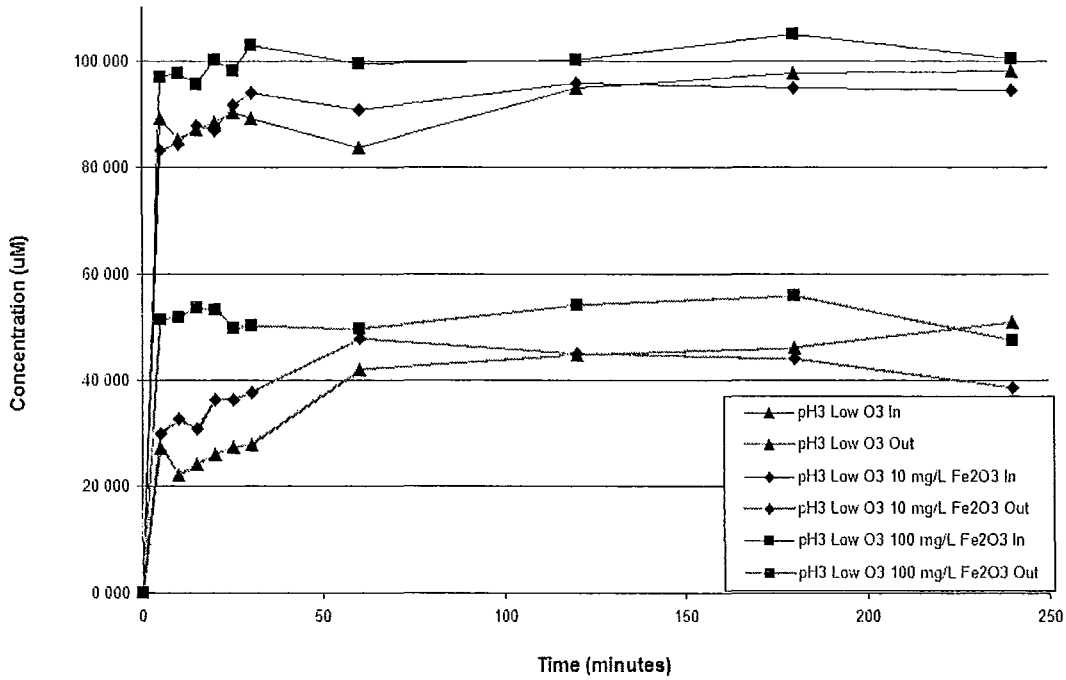

Figure B.21: Gaseous Ozone Levels for SAO Experiments

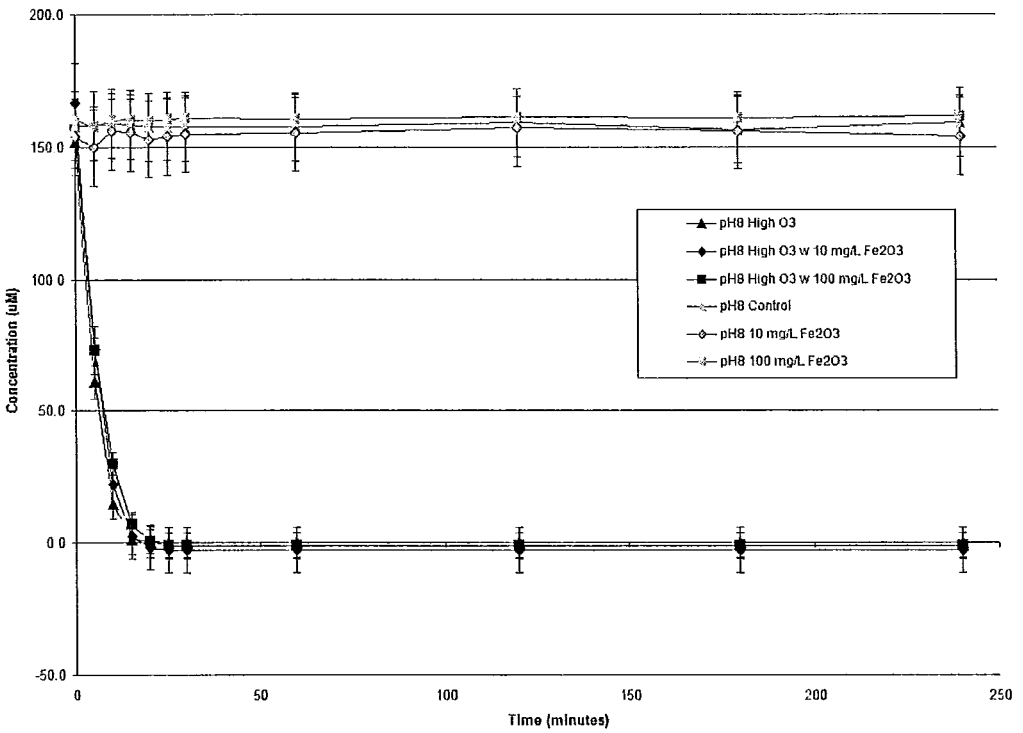

Figure B.22: SA Degradation Curves for pH 8 Potassium Phosphate Experiments

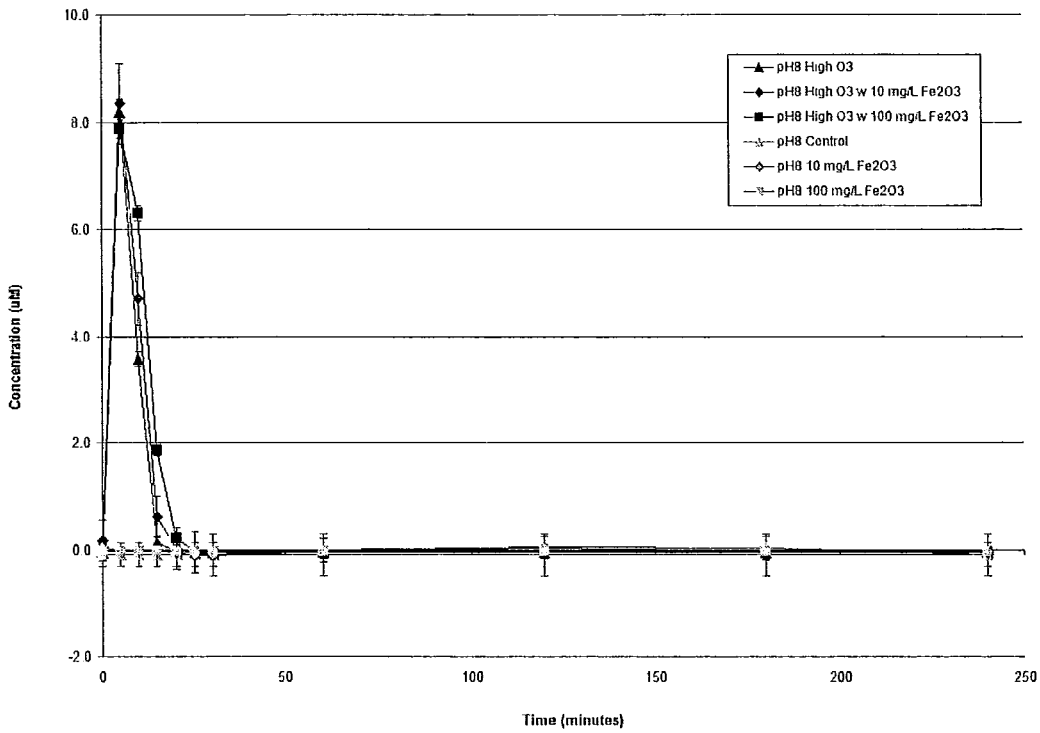

Figure B.23: 2,3-DHBA Formation for pH 8 Potassium Phosphate Experiments

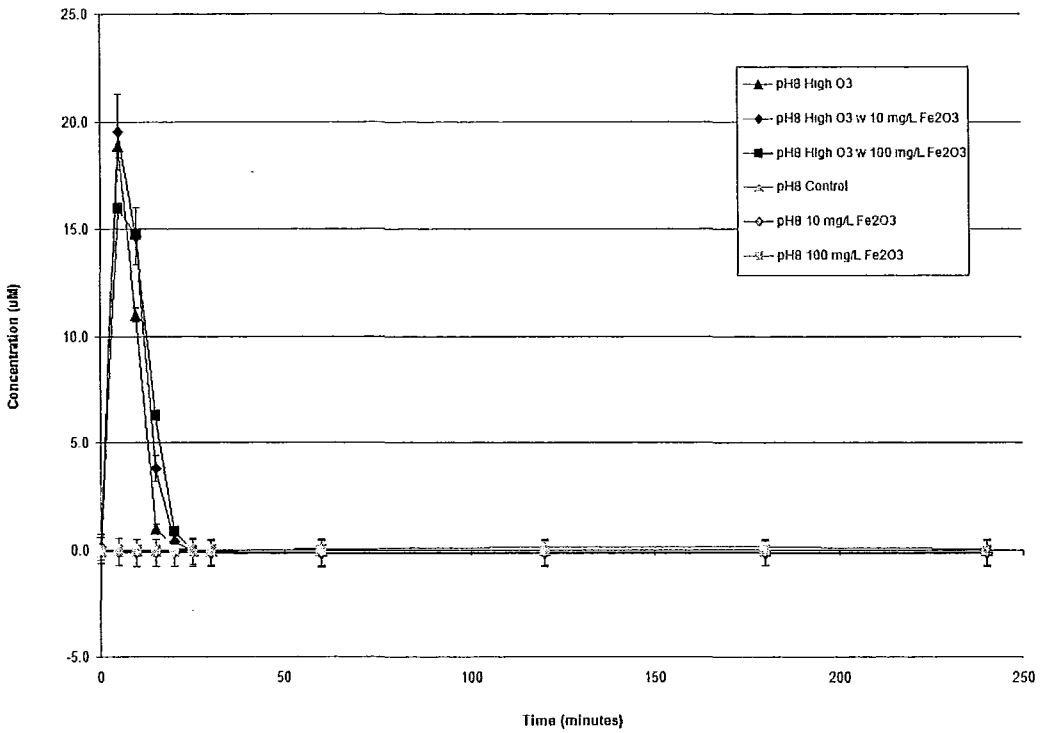

Figure B.24: 2,5-DHBA Formation for pH 8 Potassium Phosphate Experiments

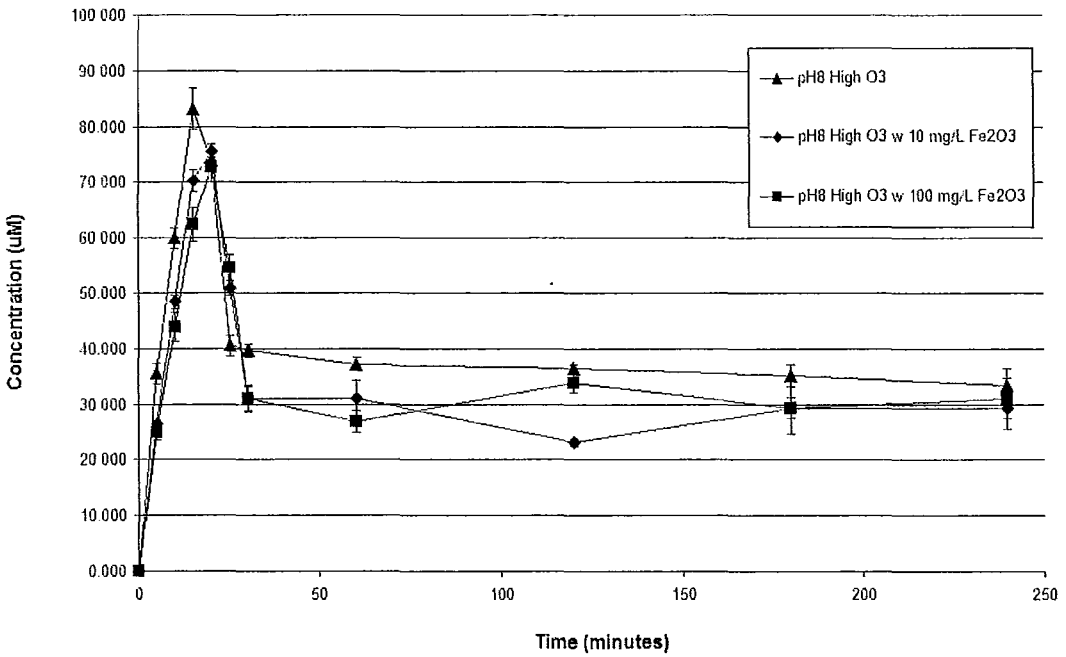

Figure B.25: Aqueous Ozone Levels for pH 8 Potassium Phosphate Experiments

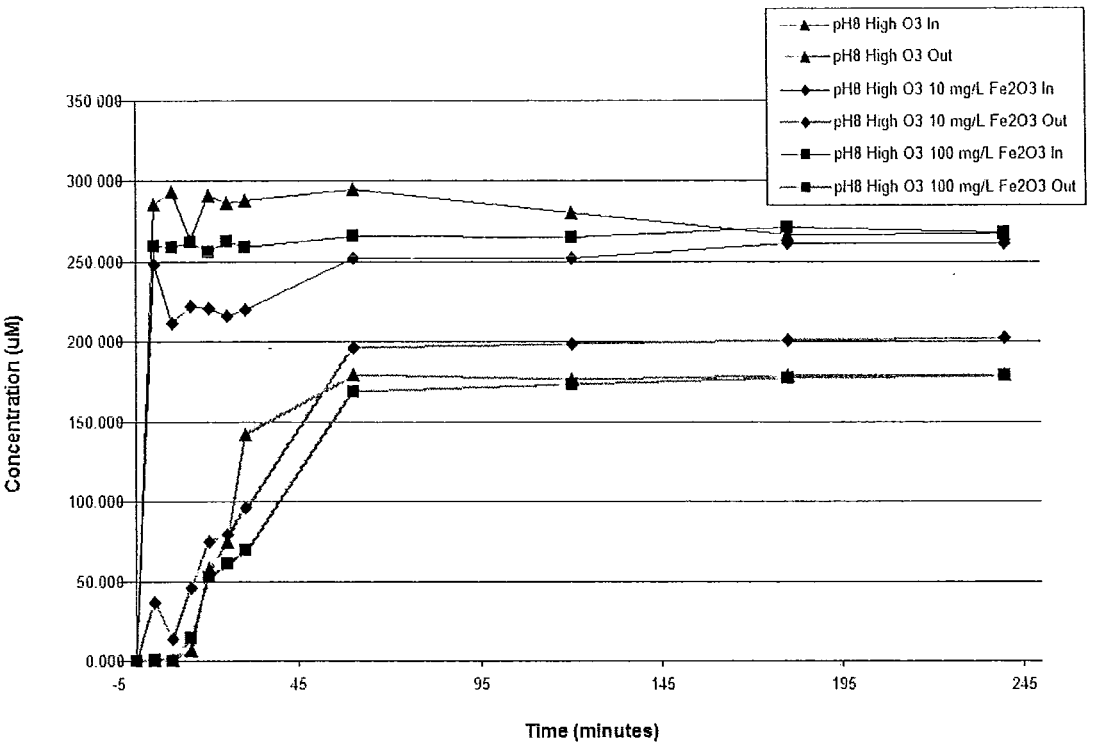

Figure B.26: Gaseous Ozone Levels for pH 8 Potassium Phosphate Experiments

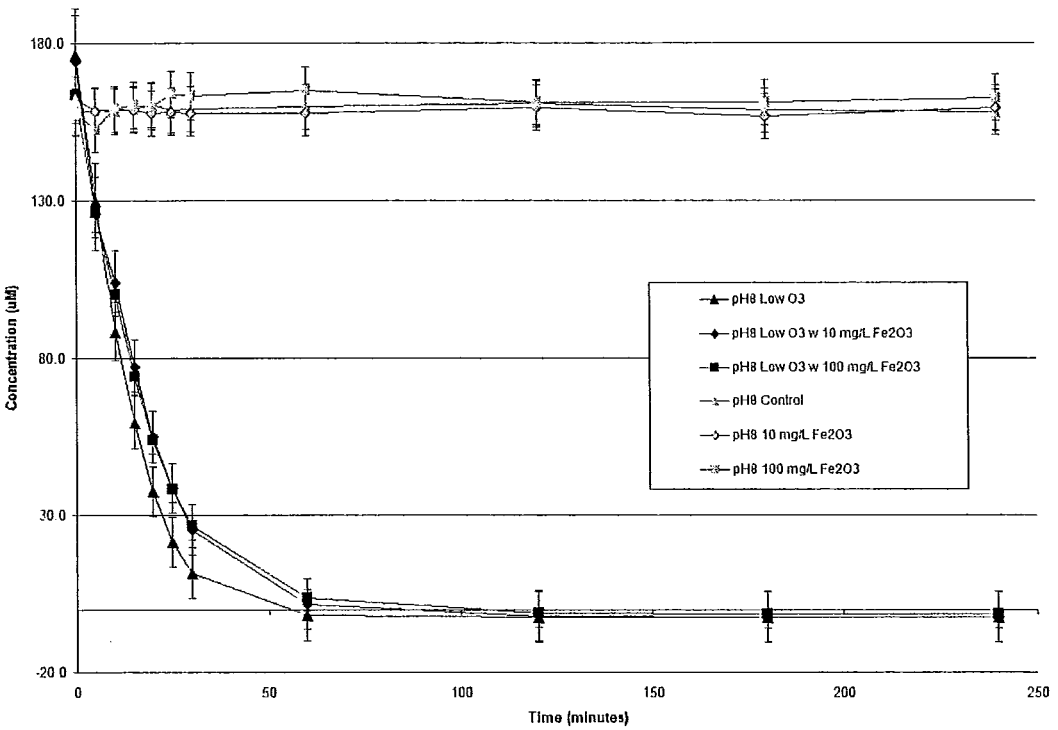

Figure B.27: SA Degradation Curves for SAO Experiments

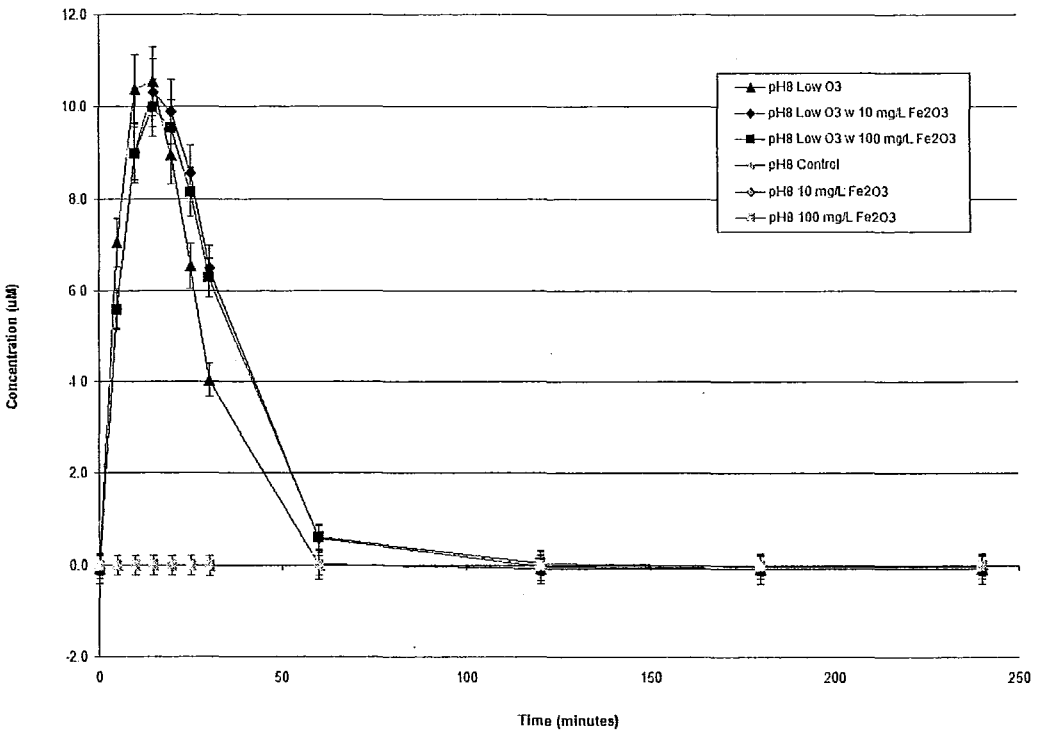

Figure B.28: 2,3-DHBA Formation for SAO Experiments

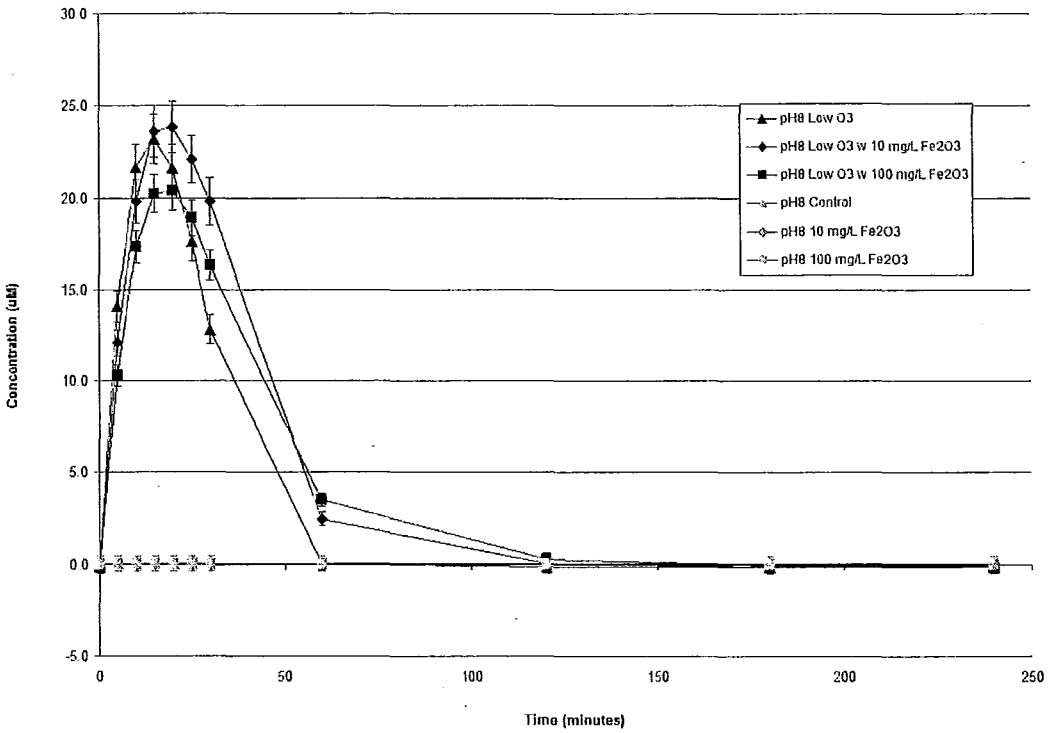

Figure B.29: 2,5-DHBA Formation for SAO Experiments

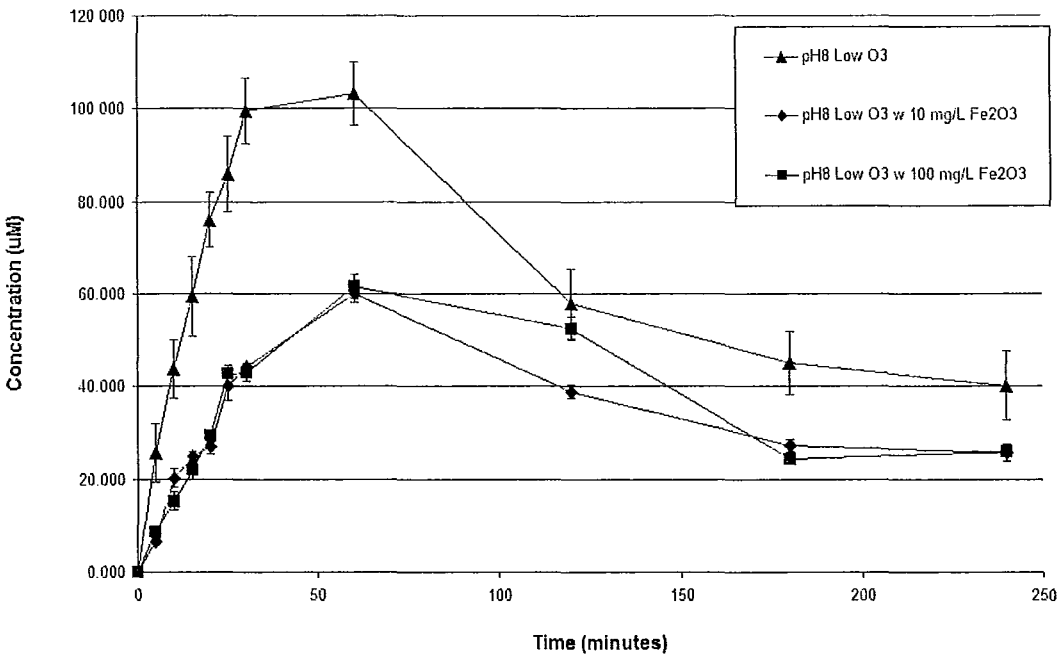

Figure B.30: Aqueous Ozone Levels for SAO Experiments

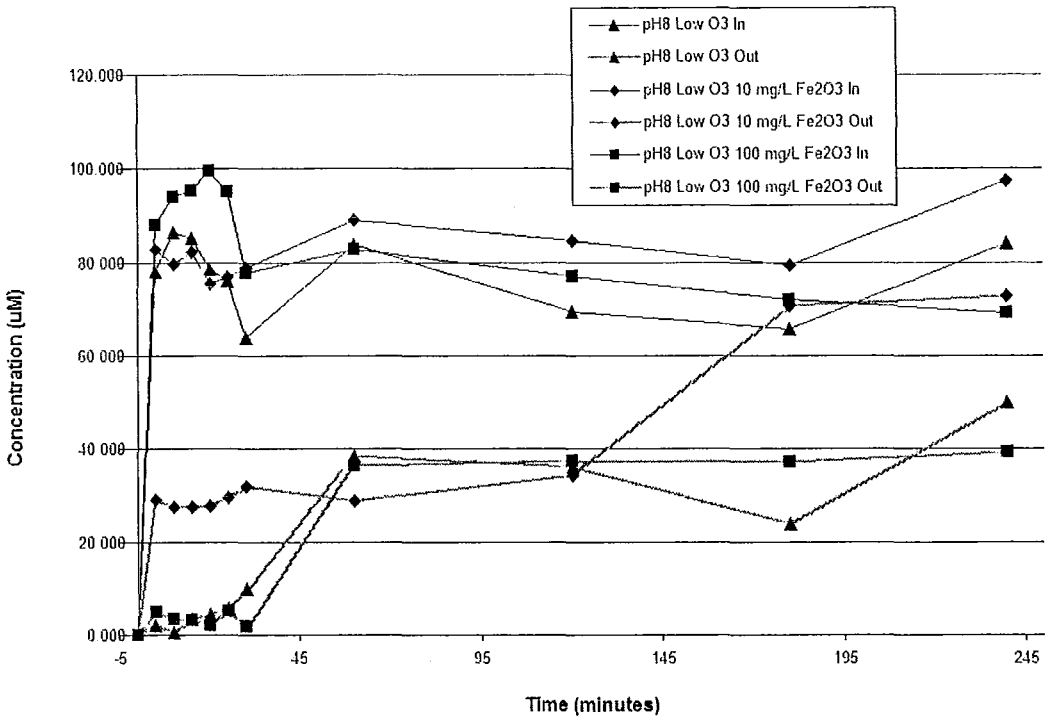

Figure B.31: Gaseous Ozone Levels for SAO Experiments

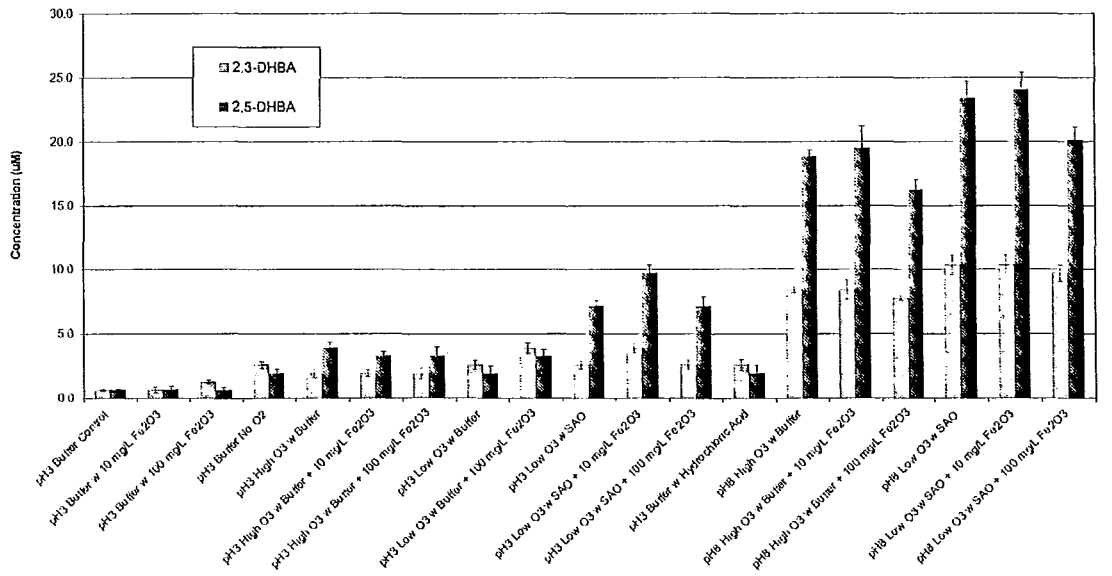

Figure B.32: Maximum Observed By-Product Concentrations

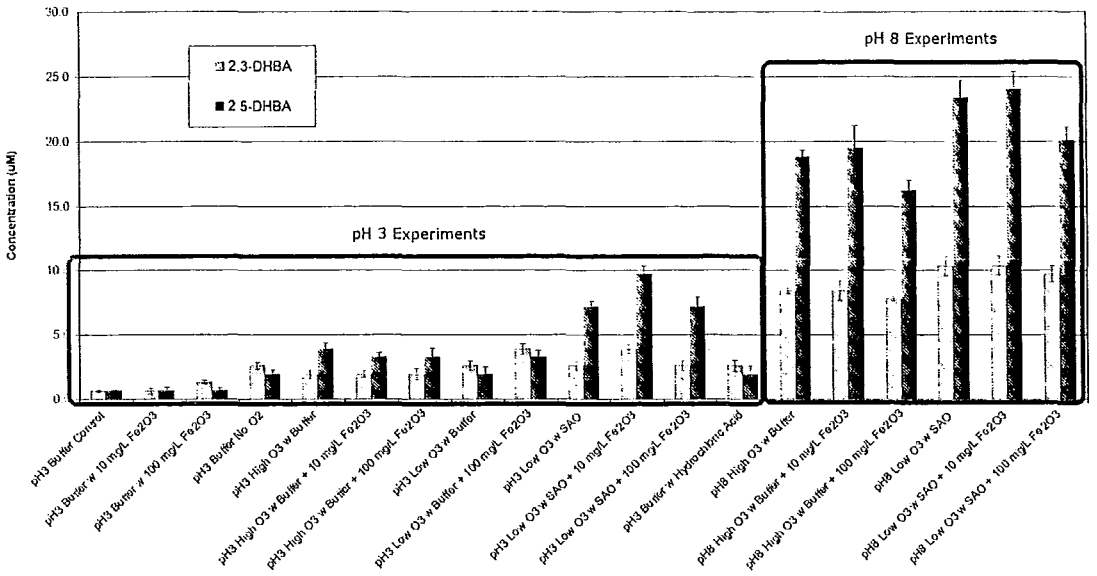

Figure B.33: Maximum Observed By-Product Concentrations

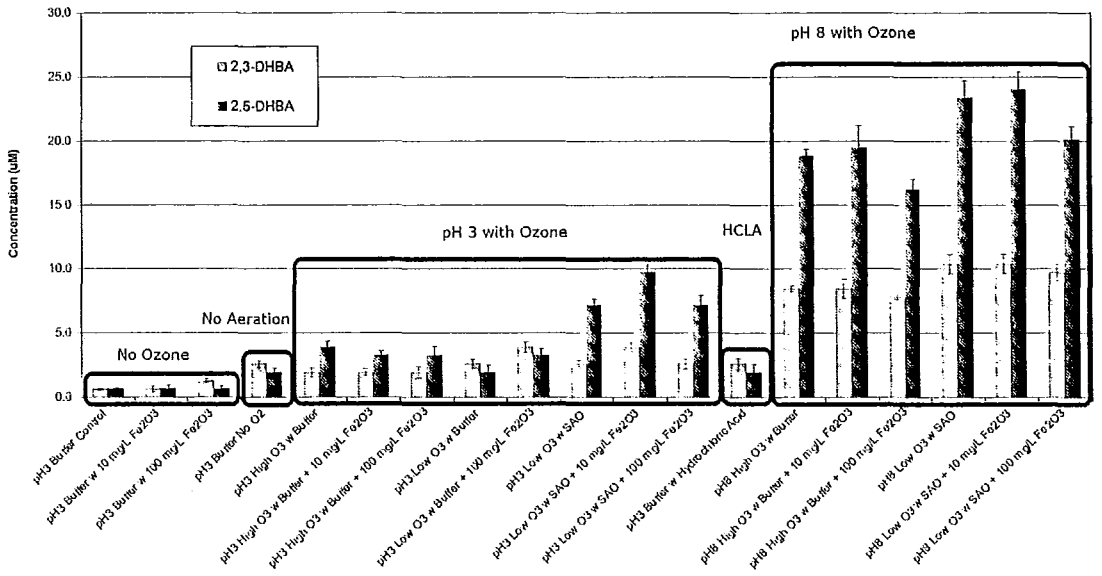

Figure B.34: Maximum Observed By-Product Concentrations

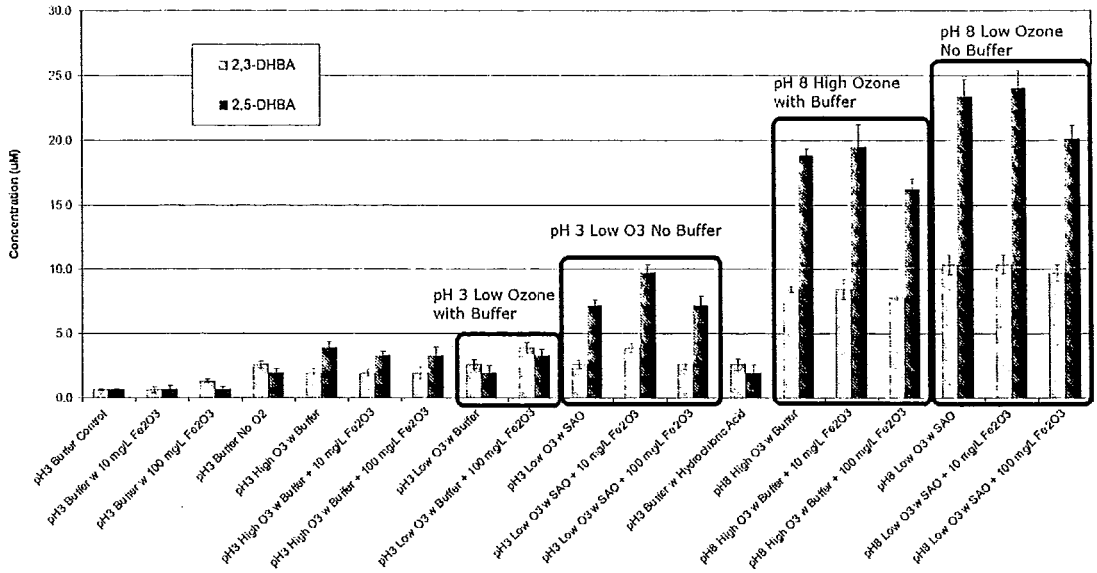

Figure B.35: Maximum Observed By-Product Concentrations

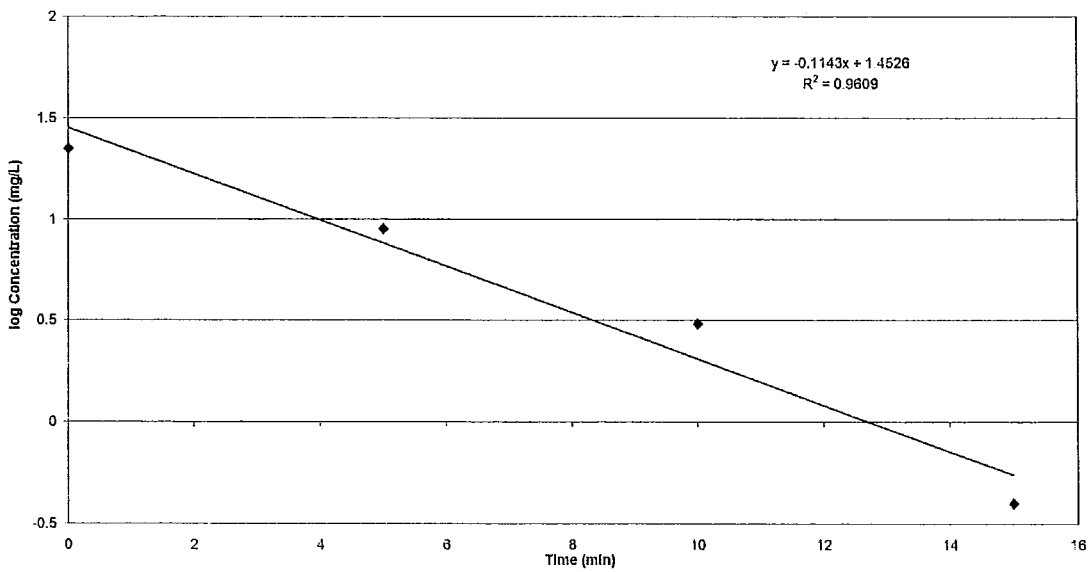

Figure B.36: Semilog Plot of SA Concentration with Time at pH 8 with Potassium Phosphate, 10 mg/L Fe_2O_3 at the High Ozone Setting